Batteries & Supercaps

Review
doi.org/10.1002/batt.202200402

Chemistry Europe
European Chemical Societies Publishing

www.batteries-supercaps.org

Special Collection

Organics-MXene Composites as Electrode Materials for Energy Storage

Mi Tang,[a] Hao Sun,[a] Lun Su,[a] Yijun Gao,[a] Fu Chen,[c] Zhengbang Wang,[a] and Chengliang Wang*[b]

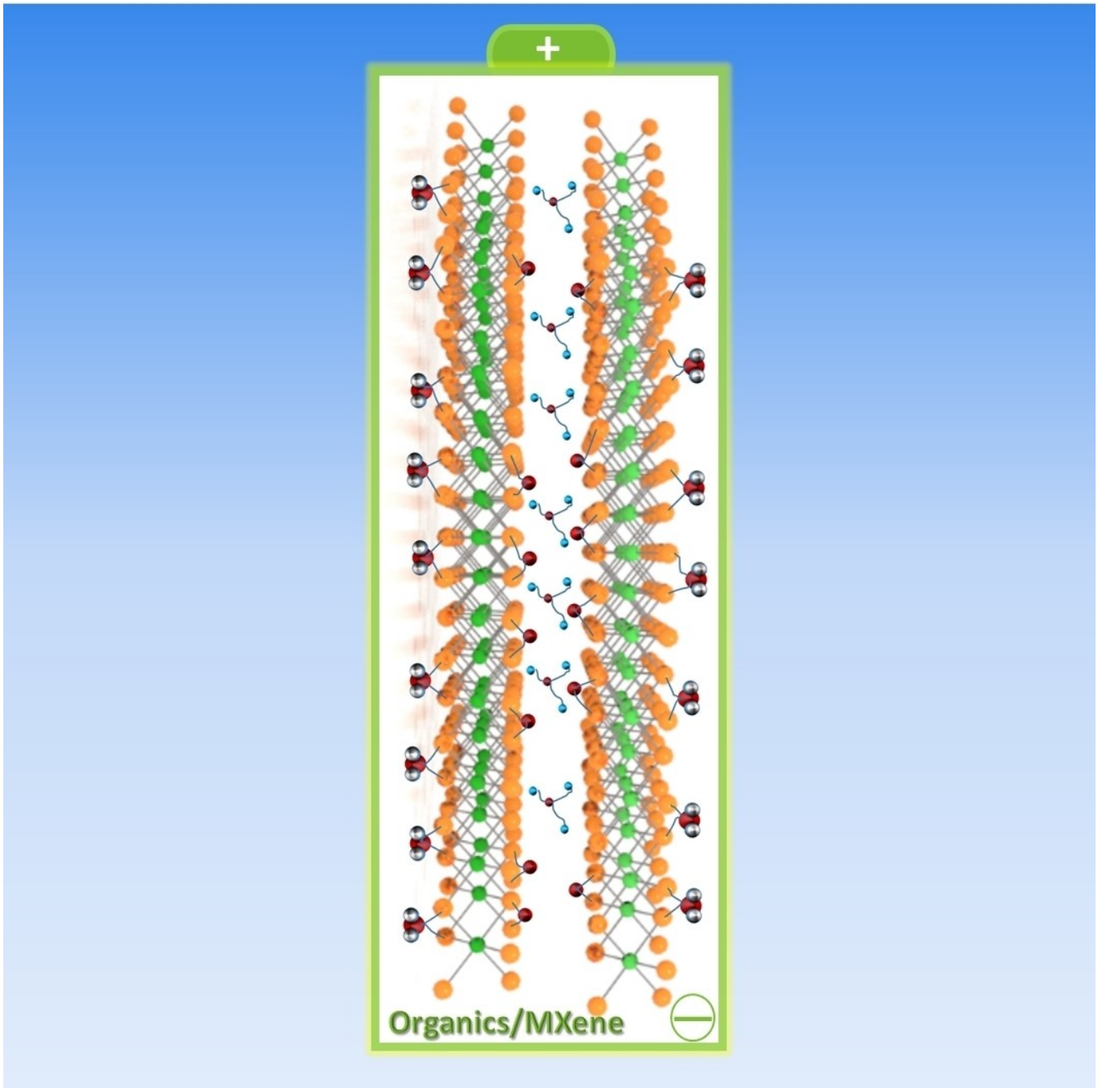

Two-dimensional (2D) transition metal carbides and/or nitrides (MXene) have emerged as a family of multifunctional materials due to the high electrical conductivity, good stability, abundant and tunable surface functional groups, showing competitive applications in energy storage and conversion. The surface functional groups and their Zeta negative potential properties facilitate the assembly of positively charged organic compounds between the MXene nanosheets to form a stable hybrid, which endow the MXene-based composite materials better electrochemical performance compared to the individual component. As such, this review exclusively highlights the development of organics/MXene-based composites and summarizes the various strategies for assembling or fabricating organics/MXene-based hybrid composites. Applications of these organics/MXene-based electrode materials in supercapacitors and batteries are also discussed in brief along with analysis of their excellent electrochemical performances and the charge storage mechanisms. Finally, some remaining challenging issues and future opportunities of organics/MXene composites as electrode materials for the high-power and low-cost rechargeable batteries or supercapacitors are also discussed.

1. Introduction

How to develop high performance energy storage system has become one of the "key scientific issues of transformative technology".[1] Although commercial lithium-ion batteries have made great development both in performances and cost, they still fall short of the requirements of "high performance energy storage batteries" in terms of safety, energy density, fast charging performance and sustainable development.[2] Access to better performance batteries calls for developing high-performance energy storage materials and deepening new energy storage mechanism as well as innovation of the new battery system. Secondary batteries based on organic electrode materials are emerging energy storage systems in recent years. The advantages of diverse structures, designability, rich resources, biodegradability and relatively mild synthesis and preparation made it promising emerging electrode materials in secondary batteries.[3]

Compared with strong ionic and covalent bond for inorganic materials, the most prominent feature of organic materials is the weak intermolecular interaction and the relatively large intermolecular spacing, which enabled the materials to store large sized and multivalent metal ions, especially of sodium, potassium and zinc ions, and other larger anions.[4,5] Organic electrode materials have developed rapidly in recent years. According to incomplete statistics, a total of nine kinds of organic electrode materials have been reported so far.[6] Although the number and types of organic electrode materials have been rapidly developed, some common issues have not been well addressed, such as low electronic conductivity, ionic conductivity and low tap-density. For example, the electronic conductivity of organic sulfide cathode material is about 5.9×10^{-13} S cm^{-1}, the radical polymer is about 5×10^{-11} S cm^{-1}, and the conjugate carbonyls, such as imide and other materials, are even as low as 10^{-15} S cm^{-1}, etc.[7] The main reason is that most organic materials lack efficient electron/ion transport channels.[8–11] Therefore, a high content of conductive additives is necessary to get satisfactory electrochemical performances.[9,12] However, the high content of conductive additives will inevitably further lead to the loss of weight energy density. How to improve the electronic and ionic conductivity of organic materials is not only an important scientific problem but also meaningful practical applications.

Referring to the methods of improving the conductivity of inorganic electrode materials, the conductivity of organic materials can be also enhanced by introducing conductive carbon network with carbon materials. This topic has been comprehensively reviewed. Transition metal carbides (MXene) are a class of new two-dimensional layered functional materials with graphene-like structure, which has attracted much scientific interest in recent years.[13] The general formula is $M_{n+1}X_nT_x$ (M is transition metal, x is carbon or nitrogen, n is an integer between 1 and 3, and T_x represents surface functional groups). The firstly prepared $Ti_3C_2T_x$ MXene has been extensively and intensively studied.[14] Compared to traditional two-dimensional materials (for instance, MoS_2, graphene, et al.), the most prominent feature of the $Ti_3C_2T_x$ MXene (hereinafter referred to as $Ti_3C_2T_x$) is the high electrical conductivity (reported[15] up to 15,000 S cm^{-1}), abundant tunable surface functional groups (–F, –Cl, –OH, –NH_2, –SH, –COOH, etc.), large and controllable layer spacing (up to about 1.7 nm) and high real density (4 g cm^{-3}).[16–19] It is widely used in gas sensing,[20,21] water purification,[22] ion adsorption,[23] catalysis,[24] electromagnetic interference shielding,[25,26] energy storage[27] and other fields.[28] Due to its good electrical conductivity, surface multifunctional groups and large layer spacing, $Ti_3C_2T_x$ offers an ideal substrate to combine with other materials, such as inorganic sulfides, transition metal oxide electrode materials, carbon materials, etc., forming $Ti_3C_2T_x$-based composite materialsl.[29–32] Currently, MXene and its composite with inorganic materials

[a] Dr. M. Tang, H. Sun, L. Su, Y. Gao, Prof. Dr. Z. Wang
Ministry of Education Key Laboratory for the Green Preparation and Application of Functional Materials, Hubei Key Laboratory of Polymer Materials, Collaborative Innovation Center for Advanced Organic Chemical Materials Co-constructed by the Province and Ministry, School of Materials Science and Engineering, Hubei University
Wuhan, 430062, China
[b] Prof. Dr. C. Wang
School of Optical and Electronic Information,
Wuhan National Laboratory for Optoelectronics (WNLO),
Huazhong University of Science and Technology
Wuhan 430074, China
E-mail: clwang@hust.edu.cn
Homepage: http://flexbatt.oei.hust.edu.cn/index.htm
[c] Dr. F. Chen
School of Information Science and Engineering
Wuhan University of Science and Technology
Wuhan 430081, China

Special Collection An invited contribution to a Special Collection on Organic Batteries.

are one of the research focuses of energy storage batteries and the relevant reviews are relatively comprehensive. However, it is noteworthy that the organic electrode materials and their MXene-based composites have been widely discussed, and related papers have been growing rapidly. But there are few relevant reviews and still a lack of systematic summary of this topic. Therefore, timely updates from distinctive perspectives would still be necessary. This review mainly summarizes the preparation of MXene, common methods of organic electrode materials/MXene composites and the latest applications progress of organics/MXene composite electrode materials in energy storage.

2. Brief Introduction and Preparation of MXenes

Since the first MXene ($Ti_3C_2T_x$) was published in 2011,[14] more than 30 kinds of MXenes have been successively studied and reported, such as $Ti_3C_2T_x$, Ti_2CT_x, V_2CT_x, Nb_2CT_x, Ti_3CNT_x, $(Ti_{0.5}Nb_{0.5})_2CT_x$, $Nb_4C_3T_x$, $Ta_4C_3T_x$, etc.[13] In general, MXene was obtained by etching the A atomic layer of the precursor MAX phase. MAX is general formula with $M_{n+1}AX_n$, wherein M represents the early transition metal; A denotes A major group element (i.e., group 13 or 14) from IIIA or IVA, such as aluminum or silicon; X stands for carbon and/or nitrogen; the value of n is 1, 2, or 3 (Figure 1). The structure of MAX is characterized by the alternating arrangement of "M" and "A" atomic layers, forming a tightly packed hexagonal layered structure with the "X" atom filling the octahedral void. The M–A bond has the characteristic of a metal bond, and the bond strength is weaker than that of the M–X bond. Therefore, choosing an appropriate etching agent could etch the A atomic layer in the MAX phase along with leaving the "M" atomic layer and "X" atomic layer, resulting in the two-dimensional $M_{n+1}X_n$ atomic crystal (called MXene).[33] The etched MXene usually has an accordion-like multi-layer structure, also known as multi-layer MXene, and the layers are connected by Van der Waals interaction. Generally, the surface of MXene has functional

Mi Tang received his Ph.D. degrees from East China University of Science and Technology (2016). During 2016–2019, he worked as a postdoctoral researcher in the group of Prof. Chengliang Wang at Huazhong University of Science and Technology (HUST). He is currently a lecturer at Hubei University. His research focuses on synthesis and characterization of organic compounds for metal-ion batteries.

Hao Sun received his B.Sc. degree from Hefei University (2020). He is currently a M.Sc. candidate at the School of Materials Science and Engineering at Hubei University under the supervision of Prof. Zhengbang Wang. His research focuses on synthesis and application of benzo-type MOFs.

Lun Su is currently a M.Sc. candidate at the School of Materials Science and Engineering at Hubei University under the supervision of Prof. Zhengbang Wang. His research focuses on metal-ion batteries.

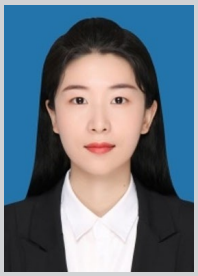

Yijun Gao received her M.Sc. degree from HUBU (2022). She is currently a Ph.D. candidate at the School of Chemistry and Molecular Science at Wuhan University under the supervision of Prof. Hexiang Deng. Her research focuses on the design of organic polymer and MXene electrodes for lithium/sodium-ion batteries.

Fu Chen received his Doctorate degree from HUST (2016). He is now an associated professor at School of Information Science and engineering in Wuhan University of Science and Technology. His research focuses on the design of microwave absorption materials and electronic functional materials.

Zhengbang Wang is currently a professor at Hubei University. He received his PhD from Karlsruhe Institute of Technology (KIT) in 2015 under supervision of Prof. Christof Wöll. Afterward, he continued working together with Prof. Wöll as a postdoctoral researcher at KIT. In 2017, he moved back to China and was appointed as Chutian Professor at Hubei University. His research interests include metal-organic framework thin films, new style porous polymer thin films, and their applications in the fields of energy and environment.

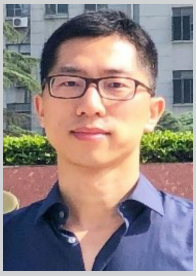

Chengliang Wang is a Professor at HUST. He received his bachelor's degree from Nanjing University in 2005 and Ph.D. degree from the Institute of Chemistry, Chinese Academy of Sciences, in 2010. He then worked at the Chinese University of Hong Kong, University of Muenster, and Technical University of Ilmenau. He was selected in the National 1000 Talents Scholars and joined HUST as a Professor in 2016. He focuses on novel conjugated organic and polymeric materials for optoelectronics and batteries.

Review
doi.org/10.1002/batt.202200402
Chemistry Europe
European Chemical Societies Publishing

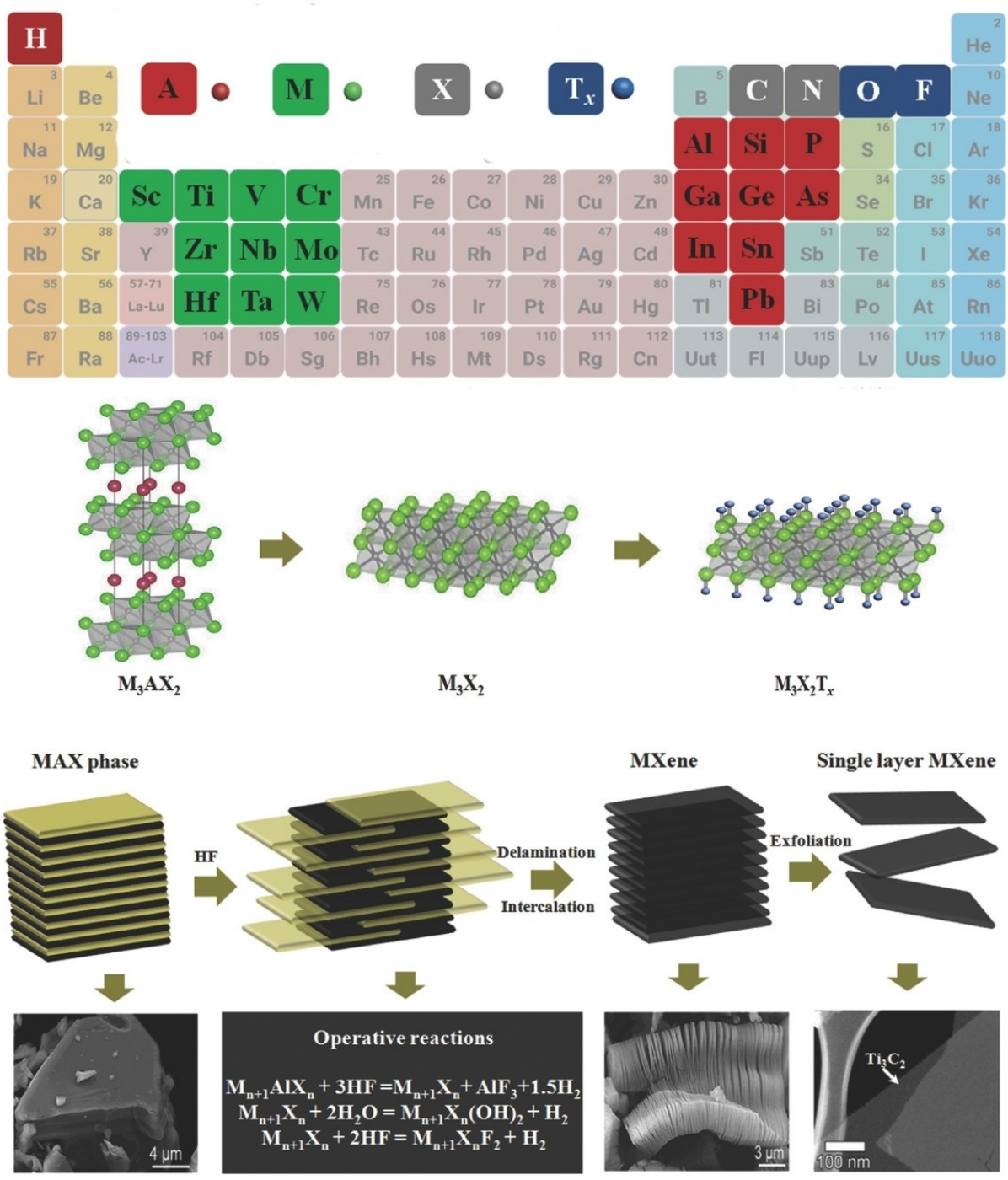

Figure 1. Illustration of the M_3AX_2, M_3X_2, and $M_3X_2T_x$ configurations, and schematic depicting the synthesis process of MXene using HF as the etchant. Adapted with permission from Ref. [35]. Copyright (2018) Wiley.

groups such as –F, –Cl, –OH, $–NH_2$, –SH, –COOH, etc., which depend on the etching agent and environment. So, it is often written as $M_{n+1}X_nT_x$, wherein T represents the surface functional group and *x* is the number of functional groups.[34]

Currently, the reported etching methods for preparing MXene included HF solution etching, in situ HF etching, molten fluoride salt etching, and fluoride-free etching. The first $Ti_3C_2T_x$ MXene was synthesized by HF solution etching. In 2011, Yury Gogotsi et al. first reported that Ti_3AlC_2 phase was etched by HF aqueous solution generating Ti_3C_2 material with two-dimensional layered structure.[14] After that, the selective etching MAX phase materials with HF solution to produce kinds of MXene has attracted great attention. Based on HF solution etching method, two-dimensional MXene materials such as Ti_2C, Ti_2N, V_2C, Nb_2C and $Mo_2Ti_2C_3$ have been successively reported.[36] This method can be described by the following reaction equation:

$$M_{n+1}AX_n + 3HF \rightarrow AF_3 + \frac{3}{2}H_2 + M_{n+1}X_n \quad (1)$$

$$M_{n+1}X_n + 2H_2O \rightarrow M_{n+1}X_n(OH)_2 + H_2 \quad (2)$$

$$M_{n+1}X_n + 2HF \rightarrow M_{n+1}X_nF_2 + H_2 \quad (3)$$

Equation (1) represents the formation of $M_{n+1}X_n$ materials from MAX, and Equations (2) and (3) represent the surface functionalization of $M_{n+1}X_n$ phase. After etching, the positions of layer A are occupied by functional groups, such as –OH, –F, and –Cl, from the reaction system, resulting in the stable state of $M_{n+1}X_nT_x$. T represents the functional groups attached to the surface of M atom.

However, it should be noted that this method has great safety risks because of the highly toxic and corrosive of HF acid. Therefore, non-HF etching methods seem more attractive. For example, $Ti_3C_2T_x$ MXene was prepared by LiF/HCl or LiF + NaF/HCl mixing solution (so-called MILD method),[33] NH_4F aqueous etching method,[37,38] Lewis acid molten salt method[39] or alkali-assisted hydrothermal method,[16] etc., respectively. For instance, Huang et al. showed the $Ti_3C_2T_x$ MXene synthesis from the reaction between Ti_3SiC_2 and $CuCl_2$ at 750 °C, which called a general Lewis acidic etching route for preparing MXenes.[39] Etching Ti_3AlC_2 to prepare $Ti_3C_2T_x$ by NaOH-assisted hydrothermal process was also a safer and environment-friendly strategy for preparing fluoride-free MXene.[16] In low-concentration hydrochloric acid solution, electrochemical etching of Ti_2AlC to Ti_2CT_x MXene was successfully demonstrated by M. J. Green.[40] Xie et al. also reported a fluorine-free etching method that Ti_3C_2 was synthesized by etching Ti_3AlC_2 with HCl solution under relatively mild conditions.[41] In addition, atomic layer deposition and chemical vapor deposition (CVD) techniques can also be used to prepare MXene.[42] This method has high cost and low yield. In general, it is still a great challenge to explore the preparation methods of low-cost, green and high-yield MXene materials.

3. Methods for Preparation of Organic Materials /MXene Composites

As mentioned above, MXene offers an ideal substrate to combine with other materials. Combining MXene materials into organics is an important strategy to improve the intrinsic properties of organic materials. At present, many methods have been developed to prepare organics/MXene composites, such as solution mixing, in situ polymerization, melt blending technology, etc. In the following sections, we will discuss these methods in detail.

3.1. Solution mixing

The solution mixing method is generally applied to polar organic materials. This is because the most of MXene materials contain hydrophilic functional groups, which are easy to interact with organic materials containing polar functional based on hydrogen bonds, van der Waals interaction, dipole-dipole interaction, etc., thus forming relatively stable composites. In this method, MXene is usually dispersed in polar solvents, such as H_2O, DMSO, DMF, NMP, and so on.[37,43,44] Meanwhile, some common commercial polymers, such as TPU,[45] polyfluorene,[46] PLA,[47] polyethylene imine,[48] perfluorinated sulfonic acid resin,[49] PAM,[50] cellulose,[51] PEO,[52] PVA,[53] PVDF[54] and polyacrylate acrylate resin,[55] are dissolved in the same solvent or another similar solvent, and then mixed with MXene dispersion solution[56,57] (Figure 2). After continuous stirring or sonication, a uniform and stable polymer/MXene composite can be formed. The other non-commercial polymers/MXene composites can be also synthesized by using this way. For example, Boota and others successfully prepared organic-inorganic PFD/$Ti_3C_2T_x$ hybrids by mixing DMSO solution of polyfluorene derivatives (PFDs) derivatives with the dispersion of $Ti_3C_2T_x$ by sonication in the same solvent.[46] Small organic materials/MXene composites can also be prepared in this way. For instance, multi-electron redox quinone-coupled viologen and pyridiniumium derivatives@$Ti_3C_2T_x$ MXene were prepared by using a self-assembly approach based on hydrogen bonding.[58]

Although the solution mixing has taken advantage of the surface multifunctional groups of MXene and the preparation process is relatively concise, there are still some issues, such as that MXene must be fully dispersed and organic materials must be dissolved. However, the soluble electrode material is more or less detrimental to the cycle stability for the batteries.

3.2. In situ polymerization

In situ growth method is generally suitable for the preparation of polymer materials/MXene hybrids.[59] In this case, monomer, catalyst, initiator, solvent, etc. are fully mixed with MXene, and then in situ polymerization reaction is carried out to form composite materials. In this synthesis process, the guest materials could be sufficiently dispersed in the MXene substrate that forms a good organic-inorganic heterogeneous interface on the MXene substrate interface, so as to exhibit good electrochemical, electromagnetic, mechanical and thermal properties[31,60] (Figure 3). For example, COFs were in situ grown on $Ti_3C_2T_x$ MXene to form organic-inorganic hybrid materials, which showed good photocatalytic hydrogen production performance.[61] Based on the adsorption of metal ions by rich groups on the surface of MXene, MOF particles were grown on the surface of MXene to construct high performance supercapacitor electrode materials.[62,63] In situ polymerization method requires good compatibility between monomers and MXene, so non-polar monomers are often difficult to infiltrate MXene to form a good interface. Therefore, surface modification of MXene is needed, such as by bonding and grafting various functional groups on MXene to improve the bonding strength of the interface.

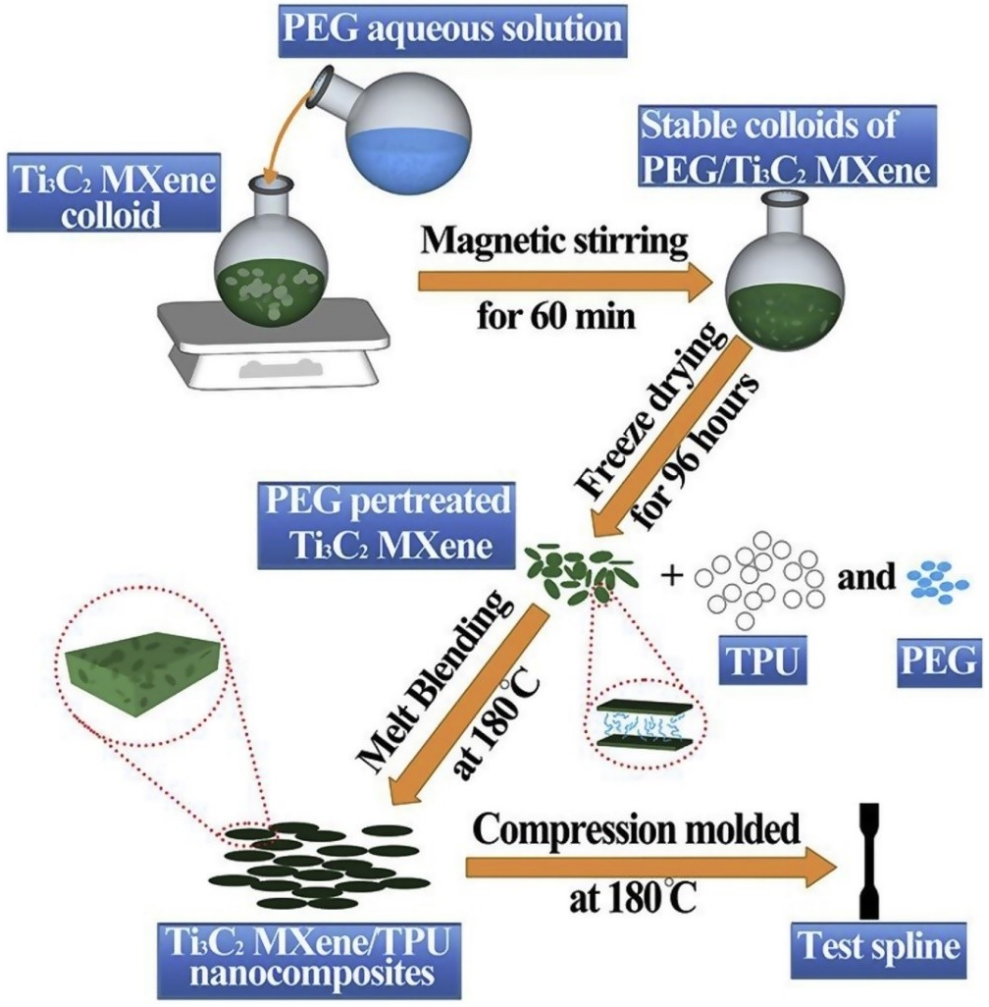

Figure 2. Typical illustration of solution mixing method for the preparation of TPU/MXene nanocomposites. Adapted with permission from Ref. [45]. Copyright (2019) Elsevier.

3.3. Melt blending

Melt blending method is the most straightforward method for good thermostability organic small molecules and polymers. Compared with organic materials, MXene has higher thermal stability. In the process of melting and blending, MXene can be mixed evenly with the fused material matrix by strongly stirring and dispersing at the melting temperature of the organic materials. In the assembly process, the interactions of functional groups play a dominant factor. Theoretically, some organic electrode materials with low melting point, such as anthraquinone (melting point is 284 °C), benzoquinone (113 °C) and TEMPO (36 °C), etc., could be used to prepare organics/MXene composites by this method. However, up to now, organic electrode materials-MXene composites were less prepared by this method. It is mainly used in some typical certain thermosetting plastics,[57,64] such polyethylene, polystyrene,[65] PANI and PVDF, etc. It should be noted that this method is only suitable for the preparation of thermoplastic polar polymer composites. When concerning non-polar thermoplastic polymer systems, surface groups of MXene needed to be modified to improve its dispersion in the matrix and interfacial bonding performance. In general, compared with the solution mixing method and in situ growth method, the MXene in some polymers/MXene composites prepared by melt blending method has better dispersion. In addition, the melt blending method is of solvent free, flexible, economical and environmentally friendly.

4. Organics/MXene Composites as Electrode Active Materials for Energy Storage

As mentioned above, MXenes are of good electrical conductivity, multi-functional surface groups and large layer spacing. Organic molecules generally contain one or more functional groups. For example, conjugated quinone electrode materials have carbonyl groups, p-type organic materials contain oxygen, nitrogen, sulfur and other heteroatoms,[66] and conjugated coordination polymer electrode materials contain transition metals.[67,68] These groups or atoms could interact with the

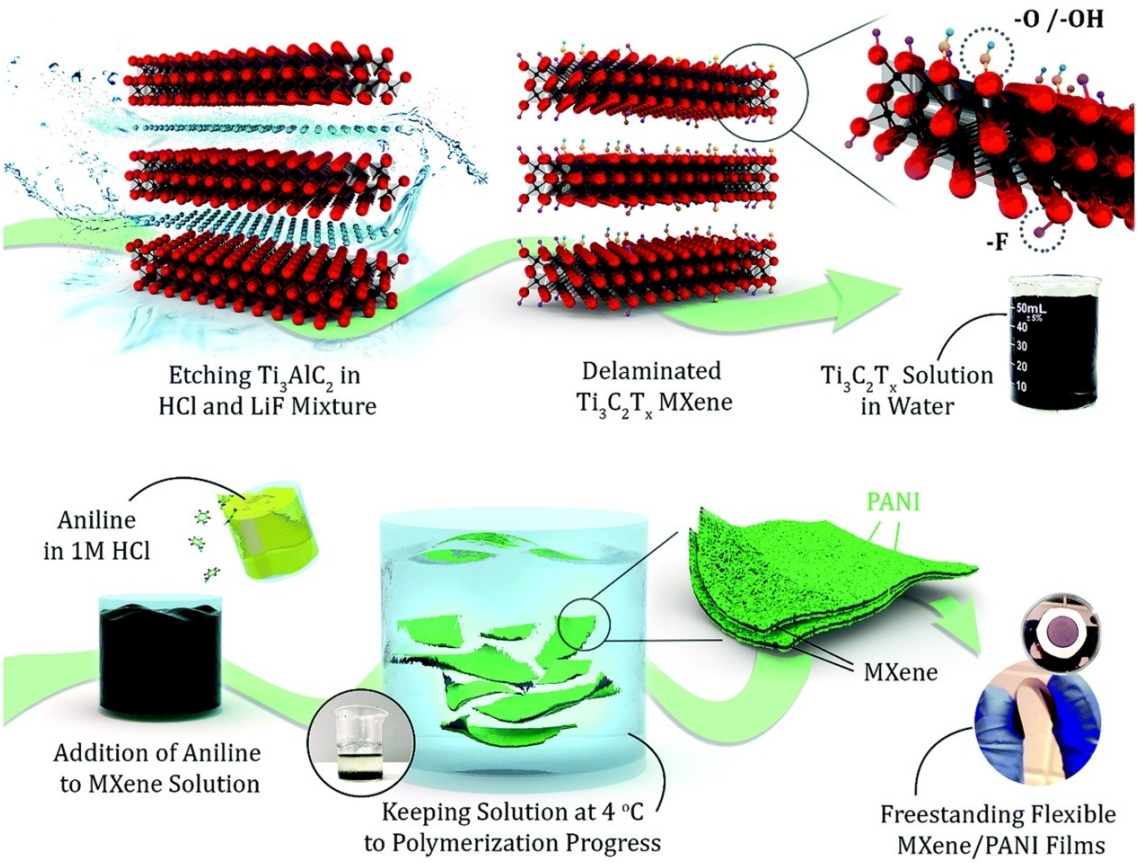

Figure 3. Typical illustration of in situ growth method for the synthesis of $Ti_3C_2T_x$/PANI hybrid electrodes. Adapted from Ref. [60]. Copyright (2018) Royal Society of Chemistry.

surface groups of MXene, such as —F, —O and —OH, etc., thus acting as assembly inductors and offering composite binding force. Therefore, the formed organics/MXene composites would bring two benefits: first, the high conductivity of MXene is conducive to improving the conductivity of organic materials, so as to improve the utilization of materials; second, the surface multi-functional groups and large layer spacing contribute to adsorption of electrolyte and facilitating ion transport. In view of this, combining suitable MXene with organic electrode materials to form organic-inorganic hybrids is a kind of advantageous strategy to improve the electrochemical performance of organic materials. Therefore, in this part, we summarized the development of organics/MXene composites in energy storage systems, mainly concerning the supercapacitors and secondary batteries. At the same time, based on recent advances and our research, the related energy storage mechanism is also discussed.

4.1. Organics/MXene composites as electrode active materials for supercapacitors

As early as when $Ti_3C_2T_x$ MXene was firstly developed, it was used as the electrode material for the supercapacitor.[69] However, the Van der Waals forces make MXene nanosheets tend to restack, which hinders the ion diffusion kinetics and further reduces the capacitance. Ions or molecular intercalation could make for the advance of in solving this problem. For instance, after the intercalation of some ions, such as Li^+, Na^+, Mg^{2+}, K^+, NH_4^+, or Al_3^+ ions, the flexible $Ti_3C_2T_x$ MXene paper electrodes showed high volumetric capacitance of up to 350 F cm^{-3} in NaOH solution.[69] This high volumetric capacitance was much higher than that of commercial activated carbon electrodes (about 60–80 F cm^{-3} in organic electrolytes) and comparable to the best graphene-based electrode materials available at the time. The ultra-high volume capacitance was attributed to the pseudocapacitances from the redox reaction on the surface groups of MXene. The MXene-based electrodes in aqueous electrolyte show the insertion of hydrated cations, and hydrated cations form a double electrical layer in one layer of interlayer space of MXene. Therefore, optimizing the spacing between MXene layers is beneficial to improve its pseudocapacitance properties.

Organic/MXene composites provide another possible solution based on the synergetic effect. The surface groups of MXene make it exhibit hydrophilic characteristics. At the same time, MXene has negative Zeta potential, which can induce orderly assembly of organic molecules with MXene based on electrostatic interaction, especially in the interlayer assembly. Therefore, organic molecules with different polarity can self-assemble with MXene under certain conditions to realize the regulation of MXene layer spacing. By using solution mixing, as

shown in Figure 4, Yury Gogotsi and co-workers prepared three organic-inorganic PFD/$Ti_3C_2T_x$ hybrids based on the host-guest interaction.[46] Because of the stronger the interaction between polar polymers with charged nitrogen containing ends (P3) and $Ti_3C_2T_x$ MXenes layers, polymer chains of P3 were aligned and well-confined between the highly conductive $Ti_3C_2T_x$ layers, which resulted in an increase in interlayer spacing and improved ionic and electronic transport. Therefore, P3@$Ti_3C_2T_x$ hybrid film electrode showed higher capacitance when compared with P1 and P2 hybrid electrodes. Under a scan rate of 2 mV s^{-1}, the gravimetric capacitance of the P3@$Ti_3C_2T_x$ electrodes exceeded 380 F g^{-1}, which corresponded to a volumetric capacitance of 1026 F cm^{-3}. Meanwhile, at a higher scan rate of 100 mV s^{-1}, P3 hybrid electrode also could hold a stable performance up to 10000 cycles with excellent capacitance retention. The authors deemed that this excellent electrochemical performance of the P3@$Ti_3C_2T_x$ hybrid is due to the synergistic impact of pseudocapacitive contributions of the P3 polymer and improved accessibility of the MXene surface to protons due to pillaring of the $Ti_3C_2T_x$ layers by polymer chains.

Based on the electrostatic-induced solution mixing, poly-(3,4-ethylenedioxythiophene)-polystyrene (PEDOT-PSS), a typical conducting polymer, could effectively produce a $Ti_3C_2T_x$/polymer hybrid film electrode via handy solution mixing and filtering (Hereinafter denoted by $Ti_3C_2T_x$/PEDOT:PSS).[70] By directly mixing a PEDOT:PSS aqueous solution and $Ti_3C_2T_x$ supernatant and followed by immersion in a concentrated H_2SO_4 solution, a flexible H_2SO_4-treated $Ti_3C_2T_x$/PEDOT:PSS hybrid film electrode was prepared. The authors proposed that the conductive PEDOT could intercalate between $Ti_3C_2T_x$ nanosheets to form a conductive bridge, which provided multi-dimensional conductive channels for fast charge transfer. As a result, the flexible $Ti_3C_2T_x$/PEDOT:PSS hybrid electrodes exhibited high volumetric capacitance of 1065 F cm^{-3} at 2 mV s^{-1} with superior rate performance in 1 M H_2SO_4 electrolyte.

Other typical conductive polymers, such as polypyrrole (PPy) and polyaniline (PANI), also work well with MXene to inform organic-MXene composites. By in situ polymerization of pyrrole in a colloidal solution of delaminated $Ti_3C_2T_x$, PPy chains were intercalated into the $Ti_3C_2T_x$ layers and well aligned between the MXene layers (Figure 5a).[71] Gogotsi et al. speculated that hydrogen bonding probably plays a key role in this alignment process. The –NH group of the pyrrole ring was hydrogen bond donor and the surface terminal groups of $Ti_3C_2T_x$, such as oxygen, fluorine or nitrogen, acted as hydrogen bond acceptors. These organic-inorganic hybrid hydrogen bonds were helpful in alignment of the PPy polymerized chains (Figure 5b and c). Therefore, the aligned PPy between $Ti_3C_2T_x$ layers expanded the layer spacing of $Ti_3C_2T_x$ MXene and, in turn, MXene also improved the electrical conductivity of PPy, resulting in better ion transport and fast reversible redox reactions. Thus, the PPy/$Ti_3C_2T_x$ film delivered a specific capacitance of 416 F g^{-1} at 5 mV s^{-1} and showed good long-term stability at 100 mV s^{-1}. So far, PPy@MXene nanocomposites have been extensively studied by using different assembly methods and shown improved power density properties, cycling stability or the volumetric capacitance in kinds of electrolytes, which have systematically documented in the recent review.[72] Herein, it will not be further discussed in detail.

Obviously, this strategy could be also applied to other organic materials to synthesize intercalated organics/MXene composites, such as polyaniline (PANI). Through oxidant-free in situ polymerization of PANI on the surface of MXene sheets, various thicknesses PANI@$Ti_3C_2T_x$ hybrid electrodes were prepared.[60] The deposition of PANI enhanced ion transport of

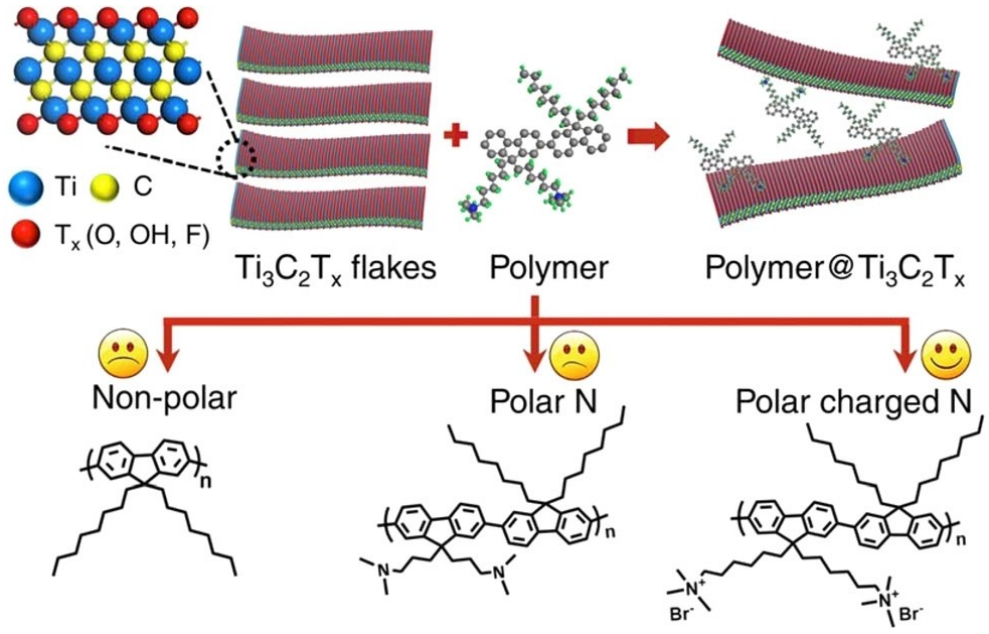

Figure 4. Schematic illustration of interaction of the polymer with $Ti_3C_2T_x$ layers (top) and the synthesized polymers with nonpolar, polar, and polar charged nitrogen lateral chain ends (bottom). Adapted with permission from Ref. [46]. Copyright (2017) American Chemical Society.

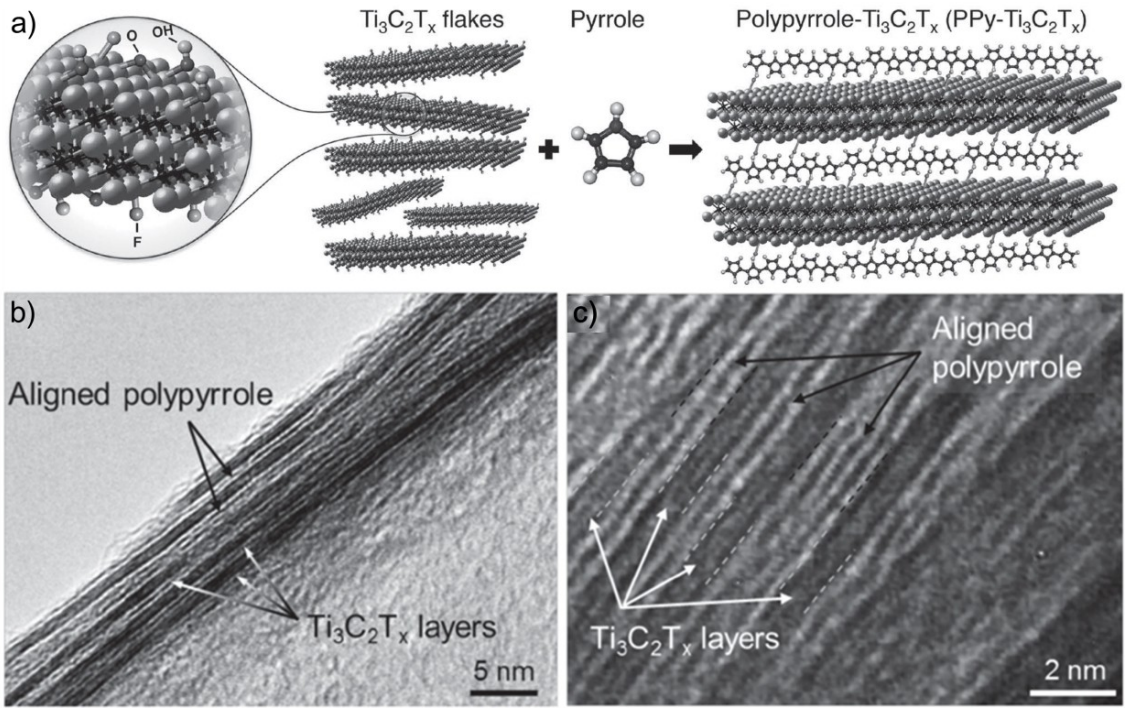

Figure 5. a) Schematic illustration of pyrrole polymerization using MXene. The terminating groups on the latter contribute to the polymerization process. b, c) Cross-sectional TEM images of aligned polypyrrole chains (bright layers) between MXene sheets (darker layers). Adapted with permission from Ref. [71]. Copyright (2016) Wiley-VCH.

hybrid electrodes while also enlarged interlayer spacing of $Ti_3C_2T_x$. It should be noted that as a conductive polymer PANI was electrochemically inactive without charge storage in the fabricated electrodes, however, improved the ionic and electronic conductivity. Thus, the thin PANI@$Ti_3C_2T_x$ hybrid electrodes delivered outstanding gravimetric and volumetric capacitances as high as 503 $F g^{-1}$ and 1682 $F cm^{-3}$, respectively. The authors speculated that the in situ assembly mechanisms of deposition of PANI on the surface of $Ti_3C_2T_x$ sheets involved the charge transfer induced polymerization mechanism, which was similar to the polymerization of EDOT on the surface of MXene.[73]

Compared to liquid acid or alkaline electrolytes, solid-state and ionic-liquid-based electrolytes possess safer advantages. By in situ polymerization of aniline monomers and $Ti_3C_2T_x$ MXene nanosheets in the presence of ammonium persulfate, a sandwich-like structure PANI@MXene hybrid was prepared by Jensheer Shamsudeen Seenath and Bishnu P. Biswal.[74] As the supercapacitor electrode material, besides the aqueous electrolyte, the PANI@MXene composite electrode also exhibited the specific capacitance of up to 322 $F g^{-1}$ at 0.25 $A g^{-1}$ with remarkable rate performance in the PVA-H_2SO_4 quasi-solid-state electrolyte. Even in an ionic liquid-based safe electrolyte [1-ethyl-3-methylimidazolium bis(trifluoromethylsulfonyl)imide, EMITFSI], the specific capacitance could reach a value of 98 $F g^{-1}$ at 0.5 $A g^{-1}$ and 109 $F g^{-1}$ at 5 $mV s^{-1}$ based on GCD and CV measurements under a voltage window of 3.5 V, rendering higher energy density performance. The authors inferred that the remarkable supercapacitor performance of PANI@MXene observed in different electrolytes was attributed to the synergistic effect that strong interfacial interaction between MXene and PANI and sufficient utilization of electrochemically active surface. Some similar research, such as the i-PANI@$Ti_3C_2T_x$, Lig@$Ti_3C_2T_x$ and Lig@$Ti_3C_2T_x$/i-PANI@$Ti_3C_2T_x$(5/5) composites films electrodes were assembled and showed excellent specific capacitance (310, 271 and 295 $F g^{-1}$ at a current density of 1 $A g^{-1}$, respectively) in flexible all-solid-state supercapacitors.[75] And Fengling Zhang et al. have developed a universal method for preparing high quality conjugated polymer-MXene composites by in situ electrochemical polymerization from the mixture of organic monomers and MXene without additional electrolyte.[76] Four polymer-MXene composite films: EDOT and $Mo_{1.33}C$ MXene mixture (E–M), $Mo_{1.33}C$ MXene with Pyrrole (P–M), Ti_3C_2 MXene with EDOT (E–T) or pyrrole (P–T) hybrids were successfully prepared. As electrodes in solid state microsupercapacitors (MSCs), the four polymer-based MSCs showed good capacitance and excellent rate capabilities in part on the strength of the superior electrical conductivity and fast ion transport in the 3D nanopores structure formed from in situ electrochemical polymerization. These work offered new possibilities for the preparation of MXene composite electrode materials with high operating voltage, which overcome the disadvantage of low working voltage for supercapacitors.

The most of above organic materials were conductive polymers. The intrinsic conductive properties made it acceptable electrochemical performances in most aspects even if they were not introduced into the two-dimensional conductive

MXenes, which more or less weakened the superiority of MXenes. In addition, most of conductive polymers are one-dimensional linear structure with relatively small specific surface area, which was in the absence of obvious porous characteristics and relatively sufficient electrolyte infiltration. Metal-organic frameworks (MOFs) as permanently porous material are regarded as promising electrode materials for supercapacitors owing to their advantages of large surface area, tunable pore size, devisable molecular structure and properties, and diversity pseudocapacitive redox centers. However, the relative low conductivity of traditional MOFs limits their application in high-performance supercapacitors that requires excellent conductivity. Owning to the high electronic conductivity and rich surface functional groups, MXene offered a versatile platform to regulate the electronic conductivity and capacitive performance of MOFs. In situ polymerization assembly is usually used in fabricating MOF/MXene composites. Pang et al. designed a general method to prepare uniform three-dimensional MXene/MOF composites.[62] Based on a coprecipitation reaction, Cu-BTC, Fe,Co-PBA, ZIF-8, and ZIF-67 were in situ constructed on the $Ti_3C_2T_x$ nanosheets yielding 3D $Ti_3C_2T_x$/Cu-BTC, $Ti_3C_2T_x$/Fe, Co-PBA, $Ti_3C_2T_x$/ZIF-8, and $Ti_3C_2T_x$/ZIF-67, respectively (Figure 6a). Compared with the pristine MOFs, all of MOFs/MXene electrodes showed higher specific capacitances owning to the improved conductivity, additional pseudocapacitive contribution of MXene and better transport of electrolytes (Figure 6b–e). Besides the familiar contributions of high electrical conductivity and extra faradaic capacitances, the surface functional groups of MXene also could act as nucleation sites for inducing growth of MOF particles. For example, the –OH group on the surface was regarded as the structure-directing agents to tune the morphology of Ni-MOFs into 2D microbelts.[77] This two-dimensional structure enabled MOF to expose more redox sites and shorten ion transport distance. Therefore, the resulting 2D Ni-MOFs/$Ti_3C_2T_x$ hybrid electrode showed a high capacitance of 1124 F g^{-1} at a current density of 1 A g^{-1} with 62% retention of 697 F g^{-1} at 20 A g^{-1}.

The other framework materials, covalent organic frameworks (COFs), have similar property with MOFs, featuring covalently-formed stable porous, well-aligned channel, high specific surface area, devisable molecular structure and accessible functional sites. Some COFs have shown advantages as promising pseudocapacitive electrodes for supercapacitors. However, it was still a challenge to explore advanced high-performance for COFs because of the poor conductivity and inaccessible redox active sites. The in situ growth of COFs on MXene nanosheets is a proven method to overcome above shortcomings. For example, anthraquinone-based COFs (AQ-COFs) were in situ constructed on the e surface of amino-functionalized Ti_3C_2 MXene nanosheets to form a series of COF@MXene heterostructure materials.[59] The authors discovered that the properties of COF@MXene heterostructure were in connection with the amounts of MXene. By adding 15 mg NH_2-MXene during the synthesis, the obtained COF@MXene-15 heterostructure delivered the best electrochemical performances (a capacitance of 290 F g^{-1} at 0.5 A g^{-1}) in 1.0 M Na_2SO_4. The synergistic efforts the redox reaction of C=O group in COF and pseudo-capacitance of MXene together contributed this high-performance supercapacitors. It follows that MXene has multiple improvement effects on MOF and COF with low electrical conductivity.

Ex-situ polymerization assembly is also a facile and efficient approach to fabricate organic/MXene composites. Yuxi Xu et al.

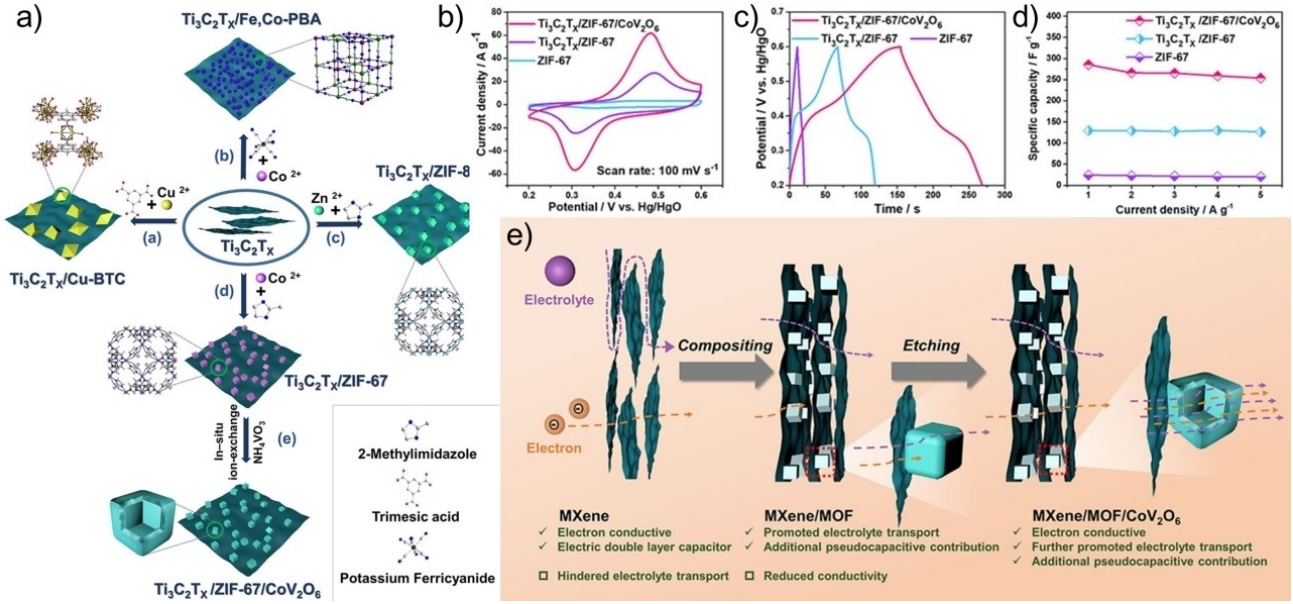

Figure 6. a) Schematic of the synthesis of $Ti_3C_2T_x$/Cu-BTC, $Ti_3C_2T_x$/Fe,Co-PBA, $Ti_3C_2T_x$/ZIF-8, $Ti_3C_2T_x$/ZIF-67, and $Ti_3C_2T_x$/ZIF-67/CoV_2O_6. b) CV curves of ZIF-67, $Ti_3C_2T_x$/ZIF-67 and $Ti_3C_2T_x$/ZIF-67/CoV_2O_6 at 0.1 V s^{-1}. c) GCD curves of ZIF-67, $Ti_3C_2T_x$/ZIF-67 and $Ti_3C_2T_x$/ZIF-67/CoV_2O_6 at 1 A g^{-1}. d) Specific capacitance of ZIF-67, $Ti_3C_2T_x$/ZIF-67 and $Ti_3C_2T_x$/ZIF-67/CoV_2O_6 at current densities from 1 to 5 A g^{-1}. e) Schematic of electrolyte/electron transport in $Ti_3C_2T_x$, $Ti_3C_2T_x$/ZIF-67 and hollow $Ti_3C_2T_x$/ZIF-67/CoV_2O_6 electrodes. Adapted with permission from Ref. [62]. Copyright (2022) Wiley-VCH.

reported hierarchical polyaniline@MXene cathode electrode prepared by casting a homogenous polyaniline layer onto a 3D porous $Ti_3C_2T_x$ MXene.[78] Unlike conventional MXenes which were usually used as negative electrodes, this PANI@F-$Ti_3C_2T_x$ heterostructure film was used as stable positive electrode and delivered an ultrahigh volumetric capacitance of 1632 F cm^{-3} at 10 mV s^{-1} and a prominent rate capability with 827 F cm^{-3} at 5000 mV s^{-1}. After constructing asymmetric supercapacitors, the PANI@M-$Ti_3C_2T_x$//M-$Ti_3C_2T_x$ supercapacitor showed volumetric energy density of 50.6 Wh L^{-1} (1.7 kW L^{-1}) and good capacity retention of 24.4 Wh L^{-1} at an ultrahigh power density of 127 kW L^{-1}. Based on the first-principal calculations, the authors proposed the PANI with larger work functions (WF = 3.46 eV) enlarged the WF of the PANI@MXene composite, which enabled MXenes to be used as positive electrode.

Electrostatic interaction is a powerful strategy to realize electrostatically self-assembly of two oppositely charged building blocks at the nanoscale.[79] As noted above, MXene has negative Zeta potential and multiple surface functionalities. In particular, the delaminated MXene nanosheets are predominantly single- or few-layered, exposing a large surface area and surface functional groups to guest molecules and thus being an ideal platform to proceed the electrostatic assembling.[31] Based-on charge transfer mechanism, Muhammad Boota et al. reported quinone-coupled viologen and pyridiniumium derivatives@$Ti_3C_2T_x$ hybrid films with multi-electron redox center, in which three organic molecules (C1, C2 and C3) were intercalated/adsorbed into $Ti_3C_2T_x$ layers. It should be noted that the authors also proposed carbonyl groups and the nitrogen sites of pyridiniumium/bipyridiniumium rings of three molecules potentially interacted with the surface groups of $Ti_3C_2T_x$ MXene via hydrogen bonding. Benefiting from strong electrostatic interactions and weak physical interactions, all hybrids were of a metallic conductive character. In a three-electrode configuration in 3 M H_2SO_4, all hybrids showed obvious pseudocapacitive character and higher capacitance above 100 mV s^{-1} compared to their pristine counterpart. Very recent similar work, the 1D/2D PANI/$Ti_3C_2T_x$ MXene nanohybrid with a high operating voltage, high specific capacitance, ultrahigh rate capability as well as good cycle stability was assembled for supercapacitors by Wenhua Hou et al. based on electrostatic interaction between negatively charged $Ti_3C_2T_x$ nanosheets and positively charged protonated PANI nanofibers.[80] The introduction of highly redox-active PANI nanofibers into highly conductive $Ti_3C_2T_x$ nanosheets and well-aligned nanostructure together contributed improved performance. Specially, the fabricated PANI@$Ti_3C_2T_x$//CPC asymmetric supercapacitor showed an ultra-wide operating voltage of 3.0 V, a maximum energy density of 67.2 Wh kg^{-1} (at 1.5 kW kg^{-1}), a maximum power density of 30 kW kg^{-1} (at 27 Wh kg^{-1}) and a capacitance retention of 80.4% after 5,000 charge-discharge cycles. In brief summary, there is no doubt that electrostatic interaction is a good self-assembly strategy. However, most of the current work has focused on the highly positive quaternary nitrogen atoms. It is still valuable to develop more types of positive central donor, such relatively weak intermolecular interaction groups CN, NO_2, CF_3 and so on, to further to enrich the variety of organic-MXene composite materials.

When organic molecules are covalently bonded to MXene, the strongest organic-inorganic interfacial bonds will be undoubtedly formed between organic molecules and MXene nanosheets. As a result, a typically sandwiching heterostructures will be formed. For instance, nucleophilic substitution condensation between hydroxyl groups of MXenes and *p*-iodophenyl diazonium salt resulted in chemically anchoring *p*-iodophenyl groups on the surface of MXene (named MXene-I) (Figure 7a). After the covalent attachment of *p*-iodophenyl to MXene, the antioxidant stability has been greatly improved. There was no obvious change after storing the MXene solution in ambient conditions for 14 days. Afterwards, the grafting *p*-iodobenzene of MXene further coupled with 2,6-dibromoanthraquinone (AQ) or 4,9-dibromo-2,7-dihexylbenzo[lmn][3,8]-phenanthroline-1,3,6,8(2H,7H)-tetraone (NDI) mixed with 1,3,5-tris(4,4,5,5-tetramethyl-1,3,2-dioxaborolan-2-yl)benzene (Bz) or tris(4-(4,4,5,5-tetramethyl-1,3,2-dioxaborolan-2-yl)phenyl)amine (TA) to yield a series of sandwich-like MXene-based conjugated microporous polymers (M-CMPs). Because of the inherit 2D architecture, high conductivity and large specific surface area of as-prepared M-CMPs, the typical M-PAQBz showed the capacitance of 190 F g^{-1} at a current density of 0.3 A g^{-1}. The analogue material M-PNDITA also reached a higher specific capacitance of 291 F g^{-1} at the same current density (Figure 7b–g).

In general, organics/MXene composites were prepared by in situ polymerization or ex situ mixing assembly methods. The ex situ mixing method is typically easy to handle but still face the unstable contact interface between the organics and MXene, especially in polymers/MXene composites. Moreover, due to the long-polymer chain length, the distribution achieved by the compounding process may be poor. The in situ polymerization method has more advantage in accomplishing a uniform distribution of the polymer on the surface of MXene.

4.2. Organics/MXene composites in batteries

In view of the various surface chemistry, large specific surface area, ultrathin 2D structure and excellent metallic conductivity, MXenes have already been demonstrated promise in energy storage. As early as in 2012, Zhen Zhou et al. have pointed out that the bare Ti_3C_2 monolayer has stoichiometric Li storage capacity (up to $Ti_3C_2Li_2$) based on the density functional theory (DFT) computations.[82] However, the most of as-prepared pristine MXene materials actually showed a relatively lower specific capacity. For example, for the first time, Gogotsi and co-workers[83] have discovered that Ti_2CT_x MXene as an anode material for Li-ion batteries only displayed a stable specific capacity of 160 mAh g^{-1} at a rate of C/10. Although a series of ameliorative studies have followed, either the lithium-ion storage performance was still relatively low or the complicated surface treatment processes were indispensable.[19,84,85] The low specific capacity and performance degradation were possibly caused by large unit molecular weight of MXene[86] or the

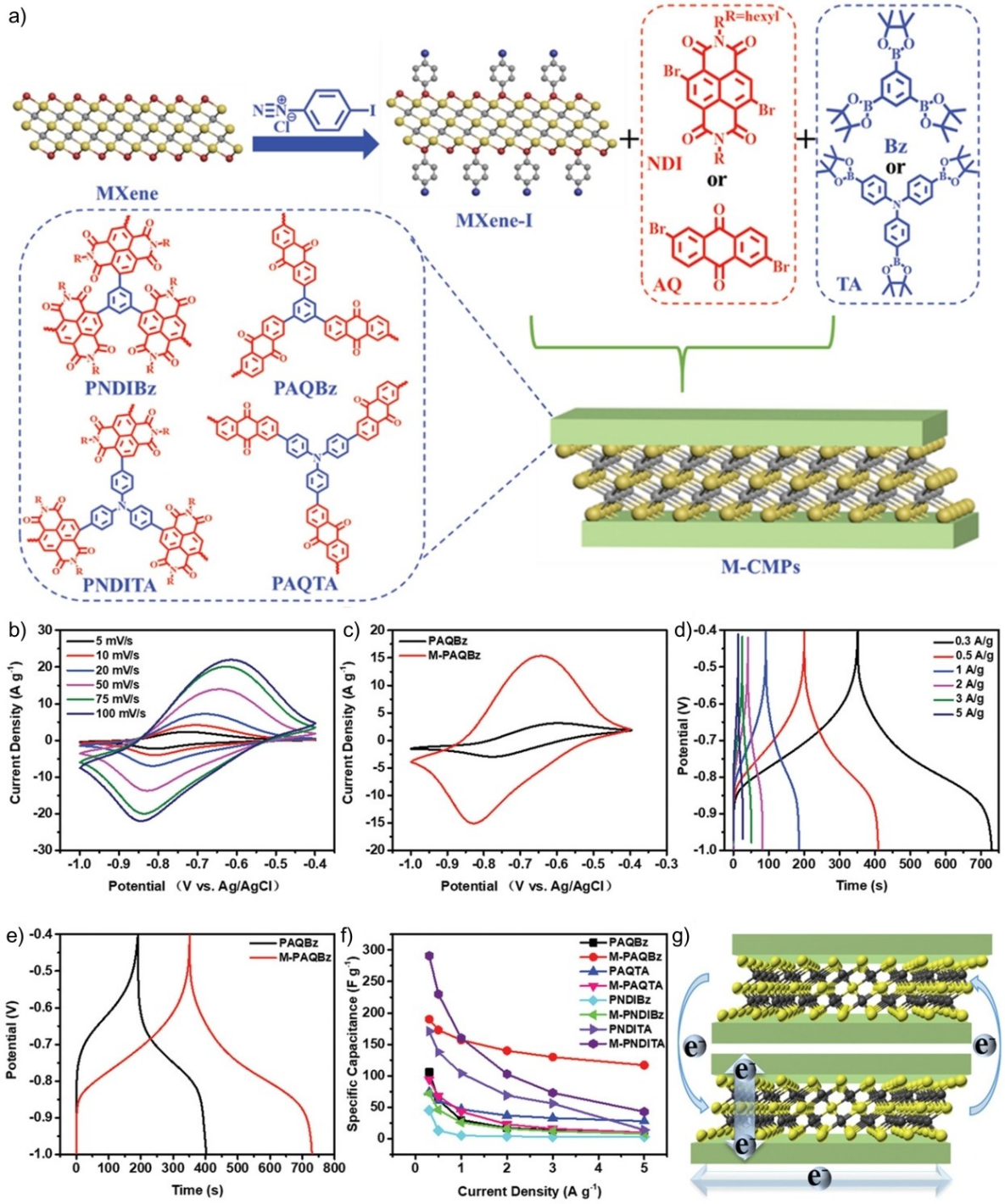

Figure 7. a) Schematic illustration of the synthetic procedures for M-CMPs. b) CV curves of M-PAQBz at different scan rates. c) The CV plots of M-PAQBz and PAQBz at 50 mV s^{-1}. d) GCD curves of M-PAQBz at different current densities. e) The GCD curves of M-PAQBz and PAQBz at 0.3 A g^{-1}. f) Rate performance of M-CMPs and corresponding CMPs at current densities ranging from 0.3 to 5 A g^{-1}. g) Schematic diagram of the charge transfer path during charging/discharging. Adapted with permission from Ref. [81]. Copyright (2020) Wiley-VCH.

surface functionalization of F and OH, which blocked Li transport and decreases Li storage capacity.[16,82] The restacking/aggregation of MXene nanosheets and susceptible oxidation were also associated with capacity degradation. It seems that bare MXene is a natural unsuitable to act as battery electrode material. Therefore, MXene is generally used as a building block to construct heterostructure with other materials, such as MoS_2, carbon materials, MnO_2 and other inorganic materials, so as to obtain better electrochemical performances. There have been a number of excellent review papers to systematically address this topic, i.e., MXene-based materials for electrochemical energy storage.[27,30,32] This paper will not repeat it. Similar to

supercapacitors, the insertion of organic molecules not only expands the interlayer spacing of MXene nanosheets, but also enhances the electrical conductivity of organic materials as well as ion transport kinetics, which significantly improve the electrochemical performances of organics/MXene composites. Hence, in this section, we mainly focus on the application of organics/MXene in the rechargeable batteries, such as such as Li-ion batteries (LIBs), lithium-sulfur batteries (LSBs), sodium-ion batteries (SIBs), potassium-ion batteries (PIBs), zinc-ion batteries (ZIBs)[87] and so on. Of course, the mentioned above methods used to prepare composite electrode materials for supercapacitors are also suitable for rechargeable batteries.

4.2.1. Organics/MXene composites as cathode materials

Even though the organics/MXene composites prepared by solution mixing assembly or electrostatic self-assembly were generally the low content of organic materials, these methods were of concise and maneuverable. Therefore, most of researchers adopted these methods to fabricate organics/MXene composites electcrodes. Jinkui Feng and co-authors designed PTCDA@MXene heterostructure via a scalable and simple electrostatic self-assembly strategy with about only 5% of PTCDA in the hybrid.[88] The authors thought that 2D $Ti_3C_2T_x$ MXene nanosheets in the heterostructure could not only improved the electronic conductivity and electrochemical kinetics of the electrode, but also inhibited the dissolution of PTCDA in the organic electrolyte. Used as LIBs and SIBs cathode materials, PTCDA@MXene exhibited better electrochemical performances than that of bare PTCDA. For instance, the discharge capacity of PTCDA@MXene in SIBs was 123.3, 114.7, 114.9, 115.5, 115.2, 110.9, and 106.3 mAh g^{-1} while bare PTCDA was 118.9, 115.8, 114.3, 112.5, 109.3, 101.7, and 85.3 mAh g^{-1}, respectively. Besides, this hybrid cathode also displayed higher capacity retention than PTCDA both in LIBs and SIBs during 1500 cycles. At a current density of 0.5 A g^{-1}, the PTCDA@MXene delivered the capacity retention ratio of 62.7% and 51.6% in LIBs and SIBs, respectively. But the PTCDA was only less than 23.5% in both of them. Similar work was reported by the same research group that free-standing $Ti_3C_2T_x$ MXene paper was used as a blocking interlayer to hinder dissolution of PTCDA.[89] The authors deemed that the MXene paper can efficiently adsorb PTCDA in the electrolyte. After adsorption of PTCDA, the MXene interlayer could act as an additional current collector to assist redox reaction of organic active material. In this process, it was not excluded that organics/MXene composite was in situ formed.

The major advantages of in situ polymerization-assembly strategy are higher organic material loading and better organic-inorganic interface. Based on it, we fabricated PAQS@$Ti_3C_2T_x$ MXene hybrid with the polymer weight content of about 77% via hydrogen bond and S–Ti interaction,[90] as described in as Figure 8. The hybrid showed typical sandwiched structure with intimate organic-inorganic contact that facilitated electrons/ions transport. Used as SIBs cathodes, the PAQS@MXene hybrid displayed outstanding Na storage performance with a high reversible capacity of 231 mAh g^{-1} at 100 mA g^{-1} and good rate capability (134.3 mAh g^{-1} at 5.0 A g^{-1}), both of which were better than that of the pure PAQS cathode. Based on DFT calculations, we speculated that the introduction of MXene efficiently reduced the adsorption energy of Na^+ and facilitates the reaction kinetics. Furthermore, this strategy could also be applied into poly pentacenetetrone sulfide (PPTS) to form PPTS@MXene hybrid with improved electrochemical performances. Other hybrids, such as PI@$Ti_3C_2T_x$ and PANI/Ti_3C_2 composites, also realized the efficient Mg^{2+} storage performanc.[91,92]

In addition to organic molecules, the lithium polysulfides could also be adsorbed by some organics/MXene composites to suppress shuttle effect. Different from the traditional sulfur host materials enabling suppressed shuttle effect, functional organics/MXene composites can not only suppress shuttle effect, but also improve electrical/ionic conductivity and provide high sulfur loading because of metallic conductive character and abundant terminal of MXene. It is generally believed that MXene can not only anchor polysulfides through interfacial Ti–S interactions,[93] but also catalyze the conversion of polysulfide based on heterogeneous interface. In addition, the combination of MXene with some functional organic molecules, such as organic porous materials, can effectively increase the content of sulfur loading. Following these preponderant advantages, various organic materials were employed to incorporate with MXene to form hybrids, which

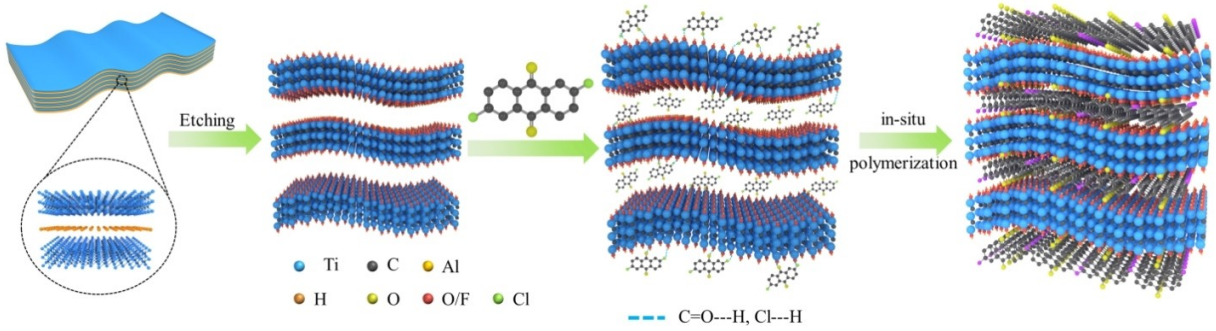

Figure 8. Schematic illustration of the fabrication of PAQS@MXene hybrid. Adapted with permission from Ref. [90]. Copyright (2022) American Chemical Society.

were used as a versatile sulfur host materials to improve lithium-sulfur batteries performance. For instance, CTF,[94] nMOF-867[95] and Tf-TAPA COF derived porous N-doped carbon[96] were combined with MXenes for advanced LSBs.

4.2.2. Organics/MXene composites as anode materials

As early as in 2012, $Ti_3C_2T_x$ MXene has been proved to store lithium ions as an anode material.[82,83] However, the pristine MXene always showed relatively inferior lithium ions storage because of the large unit molecular mass, self-stacking/aggregation and inefficient Li transport. To address these issues, organic functional materials were introduced into MXene to achieve synergistic storage of lithium ions based on the following two aspects: (1) The MXene provided conductive network; (2) Organic molecules offered more electrochemical redox site and expanded interlayer spacing of MXene through itself molecule intercalation. Hence, a sandwich-structured ordered mesoporous polydopamine (OMPDA)/$Ti_3C_2T_x$ composite as anodes through in situ assembly strategy delivered a high reversible capacity of about 1000 mAh g^{-1} at a current density of 50 mA g^{-1} along with good cycleability and rate capability.[97] This high specific capacity was much larger than that of the pristine $Ti_3C_2T_x$ MXene (225 mAh g^{-1} at a C/25 rate), showing the advantage of this strategy. The predictable advantages of polymers /MXene composites, such as highly conductive substrates, minor volume expansion, an ultrathin and stable SEI membrane outside the hybrid surface, better infiltration of the electrolyte and shortening the length for ion diffusion, conspired to contribute to the improvement of performance, the authors proposed. Due to the highly conductivity of $Ti_3C_2T_x$, the electrochemical performance of dopamine (PDA)-derived material (PDA300) was further improved[98] (Figure 9). By combining the PDA300 with highly conductive $Ti_3C_2T_x$ MXene, the resulting PDA300/$Ti_3C_2T_x$ composite exhibited excellent lithium-ions storage with high capacity (1190 mAh g^{-1}, 50 mA g^{-1}), excellent rate capability (remaining 552 mAh g^{-1} at 5 A g^{-1}), and good cycling stability (82% retaining after 1000 cycles) (Figure 9a and b), which the weight content of PDA300 was about 54.4% in the composite. Under same condition, PDA300 electrode demonstrated inferior lithium storage capacity (Figure 9c and d). The authors proposed that PDA300/$Ti_3C_2T_x$ hybrid has a higher D_{Li}^+, thus facilitating the Li^+ diffusion kinetic. Meanwhile, the introduction of highly conductive $Ti_3C_2T_x$ substrate made the composite possessed faster electron response and charge-transfer kinetics. Therefore, the hybrid electrode showed better performance. In addition, some MOF-derived inorganic-MOFs@MXene composites were also fabricated and used in LIBs and SIBs with enhanced performances.[63,99]

Intercalation of organic molecules could effectively expand the interlayer spacing of multilayer MXene. Larger layer spacing further decreased ions diffusion energy barriers and improved ion diffusion kinetics, which have been proven effective in addressing the sluggish electrochemical performances. Through the assistance of aqueous adsorption procedure, DMSO, CTAB, and PVP were intercalated between multilayer $Ti_3C_2T_x$ MXene, respectively.[100] Though all of them showed effect in increasing the layer spacing, only PVP-$Ti_3C_2T_x$ composite delivered the best lithium storage capacity, i.e., an initial reversible discharge capacity of 375 mAh g^{-1} at 50 mA g^{-1} and a stable capacity of 138 mAh g^{-1} at current density of 1000 mA g^{-1} after1000 cycles. Moreover, the CTAB- and PVP-$Ti_3C_2T_x$ composites also demonstrated sodium storage ability, albeit at a relatively low specific capacity. Likewise, the aggregated zinc methyl 3-devinyl-3-hydroxymethylpyropheophorbide a (Chl) preferred to assemble both within and on the surface of the multilayered MXene nanosheets due to the strong interfacial interaction between CHl and MXene by the simple solution-based blending-drying method. Both Ti_3C_2 MXene- and Nb_2C MXene-organic composites provided a higher discharge special capacity and a better cycle life when used as an anode material for LIBs.[101,102]

The effect of the molecule length of diacids ($HOOC(CH_2)_nCOOH$, *x*DA) on the interlayer spacing of Ti_3C_2 MXene was investigated by Yu-Lun Chueh et al.[103] Based on the dehydration condensation reaction between diacid molecules (*x*DA, $x = 2$, 4, 6, 8, 10) and teminal amino group of the $-NH_2$ functionalized Ti_3C_2, a series of *x*DA-Ti_3C_2 hybrids were prepared with unique pillar and strain structure through amide bonds (HN–C=O (Figure 10a). In the hybrid, the different lengths of diacids act as pillars to controllably expand the interlayer spacing of Ti_3C_2 layers from 1.03 to 1.45 nm. The authors indicated that the most suitable interlayer spacing for Li^+ storage capability is 1.35 nm while Na^+ is 1.38 nm, corresponding to 6DA-Ti_3C_2 and 8DA-Ti_3C_2 layers, respectively. The enlarged interlayer spacing of two hybrids boosted their metal ion (Li^+, Na^+) storage performance. The 6DA-Ti_3C_2 electrode exhibited an outstanding rate capability and long-term cycling performance with the reversible capacity of 265.7 mAh g^{-1} at 0.1 A g^{-1} after 200 cycles when it was used as LIBs anode material (Figure 10b,c). While the 8DA-Ti_3C_2 layers also showed the discharge-specific capacities of 149.8, 86.9, 59.9, 46.7, 35.4, and 22.3 mAh g^{-1} at 0.1, 0.2, 0.5, 1.0, 2.0, and 5.0 A g^{-1}, respectively in SIBs (Figure 10d and e). Besides, the 8DA-Ti_3C_2 layers were able to keep up a reversible capacity of 138.5 mAh g^{-1} after 100 cycles at 0.1 A g^{-1}. The authors confirmed that the enlarged interlayer spacing of xDA-Ti_3C_2 layers contributed the rapid Li^+/Na^+ storage dynamics thus leading to high performance.

4.2.3. Organics/MXene composites as lithium hosts

Stable and uniform Li plating/stripping without serious Li dendrites is essential to the practical application of Li-metal anode. Though the surface groups on MXenes are able to facilitate the heterogeneous nucleation of guest species (here it is Li^+), metallic Li tended to accumulate on the top surface rather than in the matrix when the bare MXene was used as a Li host probably due to limited mass transport. Ordered porous materials such as COF and MOF, have been shown to regulate ion transport, but most of COF and MOF have poor electrical

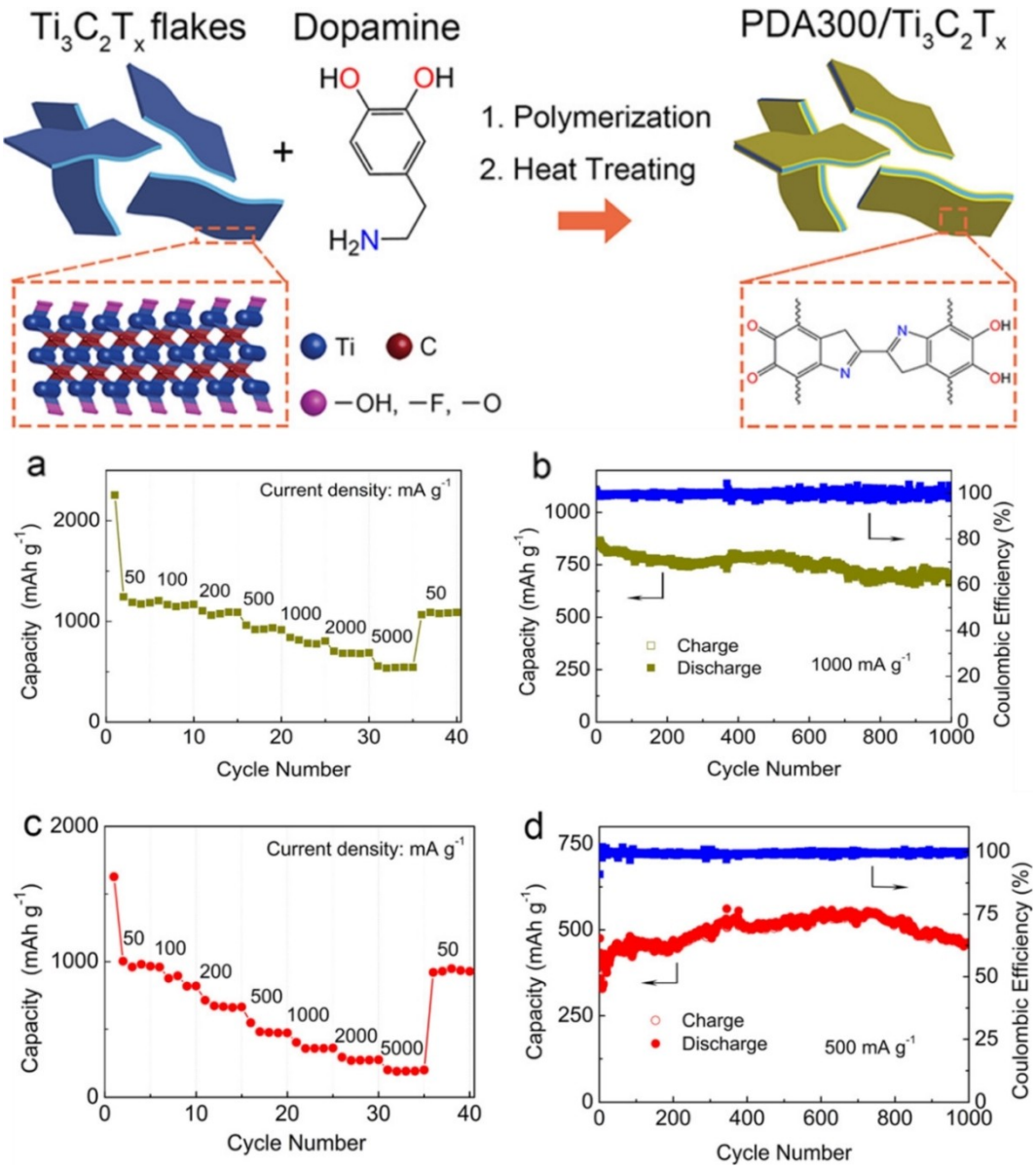

Figure 9. Top: schematic diagram of the preparation route of PDA300/$Ti_3C_2T_x$ composite. a) Rate performance of PDA300/$Ti_3C_2T_x$. b) Cycling performance of PDA300/$Ti_3C_2T_x$ at 1000 mA g^{-1}. c) Rate performance of PDA300. d) Cycling performance of PDA300 at 500 mA g^{-1}. Adapted with permission from Ref. [98]. Copyright (2018) American Chemical Society.

conductivity, which was not conducive to electron transfer. Combining MXene with COFs can incorporate complementary advantages. For instance, via a covalent assembly process, ultrathin COF-LZU was able to cooperative assemble with amine-terminated $Ti_3C_2T_x$ nanosheets, forming 2D MXene@COF heterojunction[104] that could be further processed into three-dimensional well-defined porous structure with high crystallinity and chemically stable frameworks assisted by freeze-drying (Figure 11a). This hierarchical MXene@COF monolith featured fast mass transport and charge transfer kinetics, resulting in ultralow Li nucleation/deposition overpotential (13 mV and 20 mV at mA cm^{-2}, respectively, Figure 11b), uniform and dendrite-free deposition Li deposition (reversible stripping-plating over 800 h at 3 mA cm^{-2}, Figure 11c). Both of Li–S and Li-$LiFePO_4$ (LFP) full cells assembled with the MXene@COF/Li anode delivered promising cyclability. Furthermore, a similar work, MXene/COF-LZU1 composite film was constructed by the solution mixed assembly to address the issues of Li-metal anodes (typically, uncontrollable growth of Li dendrites and unstable solid electrolyte interphase).[105] Used as Li host material, this composite film also induced effective uniform and dense Li deposition without obvious dendrite. These results implied that organics/MXene composites have promising advantages in solving the issues of lithium anode.

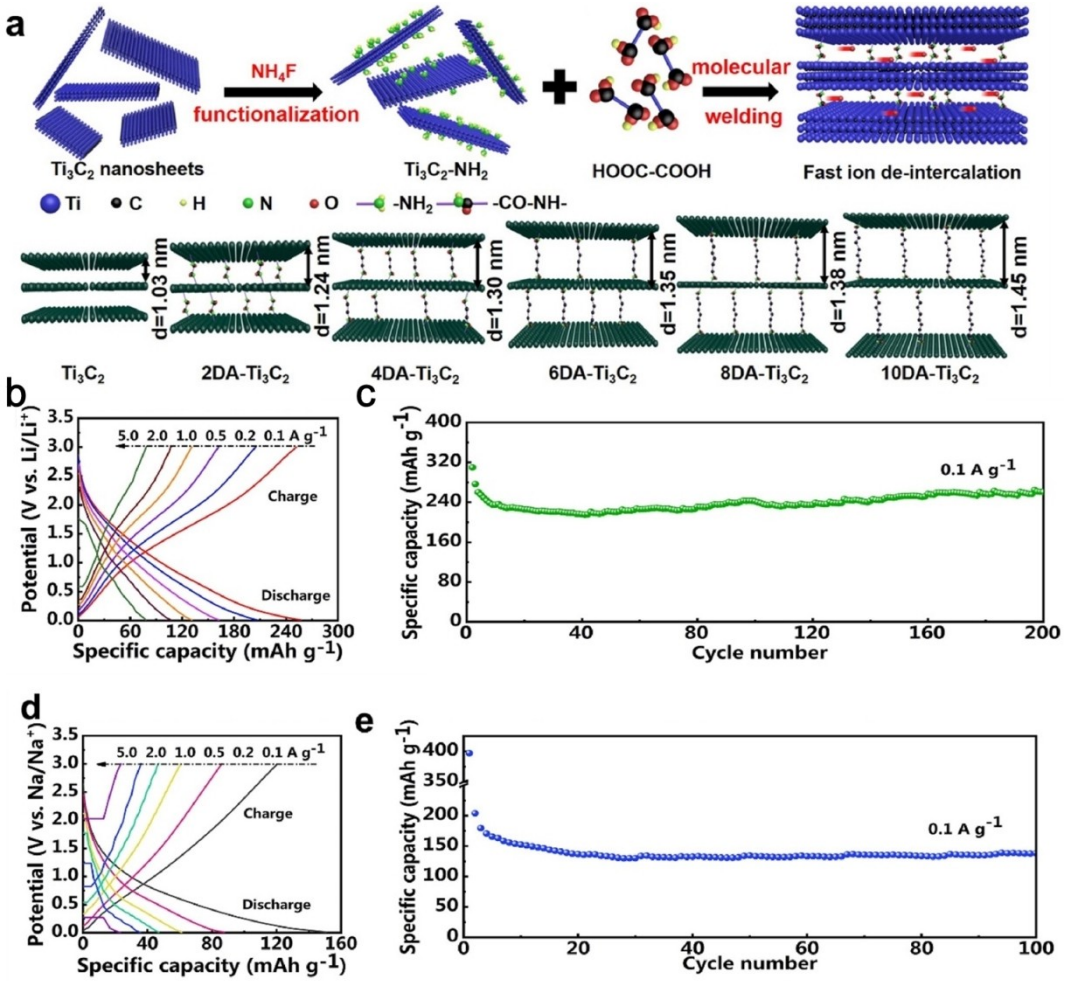

Figure 10. a) Schematic illustration for the synthesis of *x*DA-Ti_3C_2 layers. The Li^+ storage performance of 6DA-Ti_3C_2 layers: b) GCD curves at different current densities. c) Cycle stability at the current density of 0.1 A g^{-1}. The Na^+ storage performance of 8DA-Ti_3C_2 layers: d) GCD curves at different current densities. e) Cycle stability at the current density of 0.1 A g^{-1}. Adapted with permission from Ref. [103]. Copyright (2021) Elsevier.

4.2.4. Organics/MXene composites as functional modification layer for separators

Modification of commercial separators offers an effective strategy to block the migration of soluble species from the cathodes to anodes, which was widely employed to Li–S battery[106–108] and some type of organics-based batteries.[109,110] MXene has its unique advantages in not confined constructing functional modification layers, such as high electronic conductivity and abundant surface chemistry, enabling it to be widely used in LSBs.[111] However, the pristine MXene nanosheets tend to restack due to van der Waals force and the interactions between rich surface groups, which disabled the adsorption active and lowered surface area.[112] The integration of MXenes with organic materials to form composites can not only mitigate the restacking problem, but also provide more adsorption sites as well as catalyze conversion centers.[113] In generally, this composite layer was commonly used in LSBs. For instance, Xiaoju Li et al. designed the coating layer of PP separator consisting of guanidinium-based iCON uniformly loaded on Ti_3C_2 nanosheets (Ti_3C_2@iCON) through the electrostatic and hydrogen bonding interactions.[114] After etching of Ti_3AlC_2 in the aqueous solution of hydrochloric acid and lithium fluoride, the negative Zeta potential and surface functional groups of $Ti_3C_2T_x$ MXene accelerated the adsorption of triaminoguanidine hydrochloride, which further reacted with 1,3,5-triformylphloroglucinol to yield Ti_3C_2@iCON. The as-prepared Ti_3C_2@iCON nanosheets were filtered on the Celgard PP separator to generated Ti_3C_2@iCON-modified PP under vacuum. It should be noted that most of this type of modification layer was prepared by this vacuum-filtering method. Used as the separator coating layer, the Ti_3C_2@iCON film endowed CNT/S cathodes with long-term cycling stability (706 mAh g^{-1} after 2000 cycles at 2 C), high discharging capacity (1186 mAh g^{-1} after 200 cycles at 0.1 C), and good rate performance, even in the case of high sulfur loading and high rate. A series of experimental results clearly indicated that the hybrid modification layer has the following two functions: (1) Facilitating polysulfides sequestration and lithium ion conduction benefitting from the porosity and electrostatic effect of iCON; (2) The high conductivity Ti_3C_2 promoted conversion of the intercepted polysulfides based on its catalytic effects.

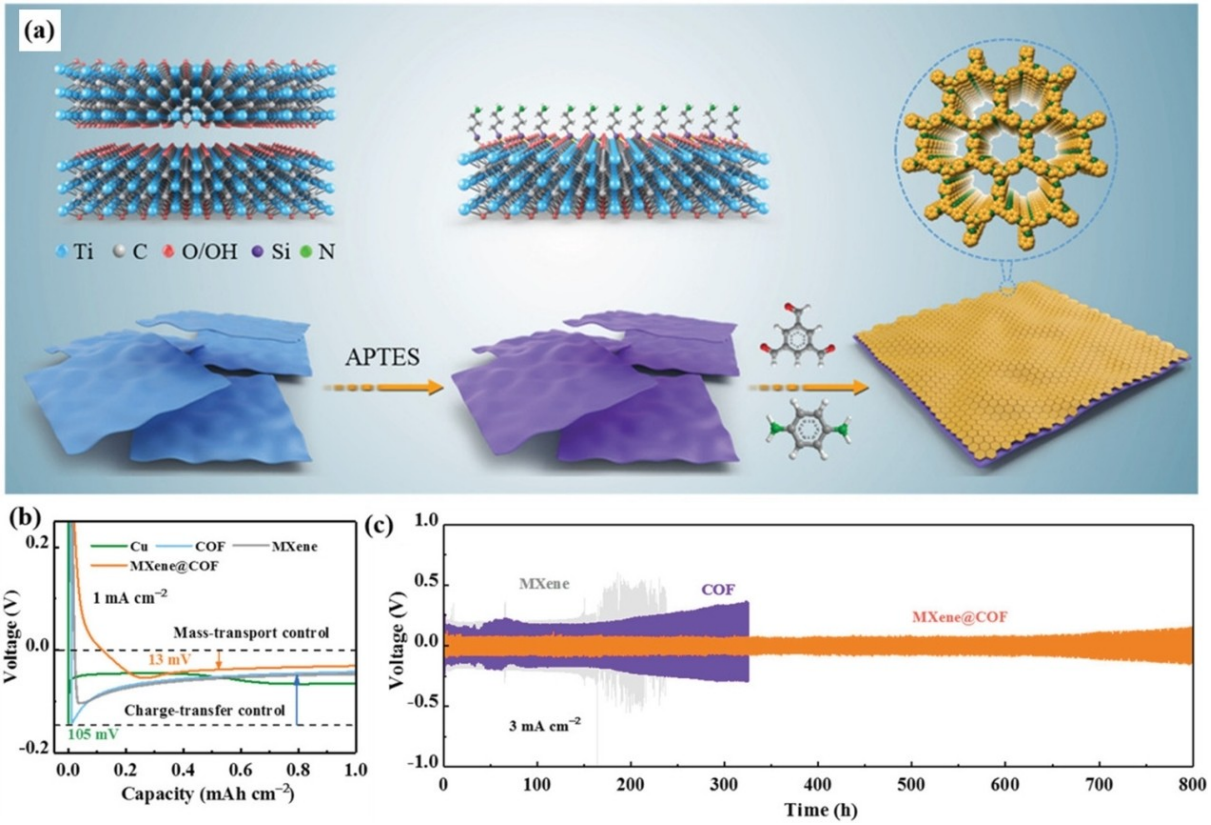

Figure 11. a) Schematic illustration of MXene covalent amination, followed by MXene@COF-LZU1 growth. b) Voltage-capacity profiles of Li deposition on the different electrodes. c) Cycling voltage profiles of symmetric cells at 3 mA cm^{-2}. Adapted with permission from Ref. [104]. Copyright (2021) Wiley-VCH.

Another work, a laminar MXene-Nafion-modified separator was prepared by a two-step process, i.e., the dispersion solution of MXene and Nafion was firstly prepared by hydrogen-bonding interactions (between the –SO_3H and –F of Nafion and –OH of MXene) and then filtrated on PP separator, generating the modified separator naming as MXene-Nafion/PP (MX-NF/PP). This functional separator significantly improved long-life cycling stability with the capacity retention of 70.1% over 1000 cycles at a higher current rate of 1 C in LSBs. The authors proposed that the synergistic effect of the physical resistance of MXene and the strong electrostatic repulsion between –SO_3^- and polysulfides together inhibited the shuttle effect. Meanwhile, the highly electrical conduction of MXene also promoted the re-utilization of polysulfides thus exhibiting the high capacities. These two examples clearly indicate that utilizing the interfacial assembly between MXene sheets and other organic materials can effectively promote the adsorption and conversion of polysulfide and achieve Li–S batter along with high specific capacity and long life.

In general, MXene or modified MXene as electrode materials (mainly as anode materials) has been widely concerned. However, so far, the organics/MXene composites as cathodes have not been get enough attention while most of the research focus on inorganics/MXene composites and their electrochemical properties. There are a variety of interactions and diverse nano-structures between organic materials and MXene, which improve the electrochemical performances of organics itself or organics/MXene hybrids in multiple dimensions. Thus, further study of these materials and their mechanisms are meaningful.

5. Summary and Perspectives

MXene is one of the most dynamic two-dimensional materials in recent years. The prominent feature of the highly electrical conductivity, tunable surface functional groups, large and controllable layer spacing, and high real density made it especially promising for applications in energy storage devices. In this review, we have introduced the recent advance and applications of organics/MXene composites in electrochemical energy storage devices, including supercapacitors, lithium-ion batteries, sodium-ion batteries, lithium-sulfur batteries, etc. The typical MXenes and their preparation methods were firstly presented. Based on various kinds of intermolecular interactions, some preparation methods for organics/MXene composites or hybrids were discussed in detail, including solution mixing, in situ preparation and melt blending. What is more, the progress of organics/MXene composites in supercapacitors and energy storage batteries was described along with their energy storage mechanisms to further in-depth understand the structure-property relationship for guiding the design of the organics/MXene-based electrodes. Despite of the noteworthy

progress, organics/MXene composite electrodes still faced some challenges and many aspects remain unclear:

1) Further developing low-cost methods for synthesizing MAX or MXene and exploring the safer and environment-friendly etching methods are necessary. In general, the current preparation of MXene mostly was concerned HF or HF-based etching method. It is noteworthy that the large safety and environmental risks, and scalable production need to be paid more attention to.
2) Precise regulation of the surface functional groups on MXene remains challenges. Overall, the surface functional groups of MXene varied with the etching method. Precision introduction of terminal groups or post modification is still relatively few.
3) Comprehensive characterization methods are still relatively insufficient. To date, the most research of surface chemistry on MXene relied on qualitative characterization methods, such as infrared spectroscopy, XPS, Raman, etc., which have been widely used to characterize the terminal groups of MXene. However, quantitative characterizations are still relatively scarce, which is very critical for the precise synthesis and in-depth understanding of the organics/MXene composites or hybrids.
4) Understanding how surface groups precisely control the assembling behavior, i.e., the interaction mechanism, between MXene nanosheets and organic molecules is still quite challenging. Admittedly, it may be extremely challenging to thoroughly investigate the mechanism based on experiments. Therefore, theoretical calculations could help us to further understand this process and guide the design of organics/MXene composites.
5) Most of the reported organics/MXene hybrid composites electrode materials have less organic components, which apparently resulted in low weight energy density for batteries. From this point, the development of hybrid composites with high organics loading is of paramount importance. However, low MXene content may cause a decrease in electrical conductivity. Therefore, a balance needs to be established between the loading and performance.
6) Finally, no matter the type of organics/MXene hybrid composites or their applications in the secondary batteries, this area just began. To this end, more efforts are needed in design and assembling techniques for organics/MXene hybrids. It goes without saying that these MXene composites will trigger broad applications.

Acknowledgements

This work was supported by the National Natural Science Foundation of China (Grant No. 21802036, 52173163, 61801186), China Postdoctoral Science Foundation (2022M710849), Hubei Provincial Natural Science Foundation of China (Project No. 2020CFB404), Department of Education of Hubei Province (Q20221004), the project supported by State Key Laboratory of Advanced Technology for Materials Synthesis and Processing (Wuhan University of Technology) and Overseas Expertise Introduction Center for Discipline Innovation (D18025).

Conflict of Interest

These authors declare no competing interest.

Data Availability Statement

The data that support the findings of this study are available from the corresponding author upon reasonable request.

Keywords: batteries · composites · MXene · organic electrode materials · supercapacitors

[1] R. Usiskin, Y. Lu, J. Popovic, M. Law, P. Balaya, Y.-S. Hu, J. Maier, *Nat. Rev. Mater.* **2021**, *6*, 1020–1035.
[2] D. Castelvecchi, *Nature* **2021**, *596*, 336–339.
[3] P. Poizot, J. Gaubicher, S. Renault, L. Dubois, Y. Liang, Y. Yao, *Chem. Rev.* **2020**, *120*, 6490–6557.
[4] S. Lee, J. Hong, K. Kang, *Adv. Energy Mater.* **2020**, *10*, 2001445.
[5] C. Wang, *Energy Environ. Mater.* **2020**, *3*, 441–452.
[6] J. Wang, A. E. Lakraychi, X. Liu, L. Sieuw, C. Morari, P. Poizot, A. Vlad, *Nat. Mater.* **2020**, *20*, 665–673.
[7] Y. Lu, J. Chen, *Nat. Chem. Rev.* **2020**, *4*, 127–142.
[8] Y. Chen, H. Li, M. Tang, S. Zhuo, Y. Wu, E. Wang, S. Wang, C. Wang, W. Hu, *J. Mater. Chem. A* **2019**, *7*, 20891–20898.
[9] M. Tang, S. Zhu, Z. Liu, C. Jiang, Y. Wu, H. Li, B. Wang, E. Wang, J. Ma, C. Wang, *Chem* **2018**, *4*, 2600–2614.
[10] C. Wang, Y. Xu, Y. Fang, M. Zhou, L. Liang, S. Singh, H. Zhao, A. Schober, Y. Lei, *J. Am. Chem. Soc.* **2015**, *137*, 3124–3130.
[11] M. Tang, C. Jiang, S. Liu, X. Li, Y. Chen, Y. Wu, J. Ma, C. Wang, *Energy Storage Mater.* **2020**, *27*, 35–42.
[12] X. Pan, P. Xue, X. Wang, F. Chen, Y. Gao, M. Tang, C. Wang, Z. Wang, *Chem. Eng. J.* **2022**, *450*, 137920.
[13] A. VahidMohammadi, J. Rosen, Y. Gogotsi, *Science* **2021**, *372*, eabf1581.
[14] M. Naguib, M. Kurtoglu, V. Presser, J. Lu, J. Niu, M. Heon, L. Hultman, Y. Gogotsi, M. W. Barsoum, *Adv. Mater.* **2011**, *23*, 4248–4253.
[15] J. Zhang, N. Kong, S. Uzun, A. Levitt, S. Seyedin, P. A. Lynch, S. Qin, M. Han, W. Yang, J. Liu, X. Wang, Y. Gogotsi, J. M. Razal, *Adv. Mater.* **2020**, *32*, 2001093.
[16] T. Li, L. Yao, Q. Liu, J. Gu, R. Luo, J. Li, X. Yan, W. Wang, P. Liu, B. Chen, W. Zhang, W. Abbas, R. Naz, D. Zhang, *Angew. Chem. Int. Ed.* **2018**, *57*, 6115–6119; *Angew. Chem.* **2018**, *130*, 6223–6227.
[17] V. Kamysbayev, A. S. Filatov, H. Hu, X. Rui, F. Lagunas, D. Wang, R. F. Klie, D. V. Talapin, *Science* **2020**, *369*, 979–983.
[18] C. Lu, A. Li, T. Zhai, C. Niu, H. Duan, L. Guo, W. Zhou, *Energy Storage Mater.* **2020**, *26*, 472–482.
[19] B. Anasori, M. R. Lukatskaya, Y. Gogotsi, *Nat. Rev. Mater.* **2017**, *2*, 16098.
[20] W. Y. Chen, S.-N. Lai, C.-C. Yen, X. Jiang, D. Peroulis, L. A. Stanciu, *ACS Nano* **2020**, *14*, 11490–11501.
[21] S. J. Kim, H.-J. Koh, C. E. Ren, O. Kwon, K. Maleski, S.-Y. Cho, B. Anasori, C.-K. Kim, Y.-K. Choi, J. Kim, Y. Gogotsi, H.-T. Jung, *ACS Nano* **2018**, *12*, 986–993.
[22] I. Ihsanullah, *Chem. Eng. J.* **2020**, *388*, 124340.
[23] M. Jeon, B.-M. Jun, S. Kim, M. Jang, C. M. Park, S. A. Snyder, Y. Yoon, *Chemosphere* **2020**, *261*, 127781.
[24] J. Peng, X. Chen, W.-J. Ong, X. Zhao, N. Li, *Chem* **2019**, *5*, 18–50.
[25] T. Yun, H. Kim, A. Iqbal, Y. S. Cho, G. S. Lee, M.-K. Kim, S. J. Kim, D. Kim, Y. Gogotsi, S. O. Kim, C. M. Koo, *Adv. Mater.* **2020**, *32*, 1906769.
[26] A. Iqbal, F. Shahzad, K. Hantanasirisakul, M.-K. Kim, J. Kwon, J. Hong, H. Kim, D. Kim, Y. Gogotsi, C. M. Koo, *Science* **2020**, *369*, 446–450.
[27] C. Zheng, Y. Yao, X. Rui, Y. Feng, D. Yang, H. Pan, Y. Yu, *Adv. Mater.* **2022**, DOI: https://doi.org/10.1002/adma.202204988.

[28] J. Zhang, S. Uzun, S. Seyedin, P. A. Lynch, B. Akuzum, Z. Wang, S. Qin, M. Alhabeb, C. E. Shuck, W. Lei, E. C. Kumbur, W. Yang, X. Wang, G. Dion, J. M. Razal, Y. Gogotsi, *ACS Cent. Sci.* **2020**, *6*, 254–265.
[29] T. Zhou, C. Wu, Y. Wang, A. P. Tomsia, M. Li, E. Saiz, S. Fang, R. H. Baughman, L. Jiang, Q. Cheng, *Nat. Commun.* **2020**, *11*, 2077.
[30] K. Li, M. Liang, H. Wang, X. Wang, Y. Huang, J. Coelho, S. Pinilla, Y. Zhang, F. Qi, V. Nicolosi, Y. Xu, *Adv. Funct. Mater.* **2020**, *30*, 2000842.
[31] C. Zhang, *J. Energy Chem.* **2021**, *60*, 417–434.
[32] P. Krishnaiah, H. T. A. Awan, R. Walvekar, S. Manickam, in *Fundamental Aspects and Perspectives of MXenes*, eds. M. Khalid, A. N. Grace, A. Arulraj, A. Numan, Springer International Publishing, *Cham* **2022**, DOI: 10.1007/978-3-031-05006-0_4, pp. 53–86.
[33] M. Alhabeb, K. Maleski, B. Anasori, P. Lelyukh, L. Clark, S. Sin, Y. Gogotsi, *Chem. Mater.* **2017**, *29*, 7633–7644.
[34] J. Halim, K. M. Cook, M. Naguib, P. Eklund, Y. Gogotsi, J. Rosen, M. W. Barsoum, *Appl. Surf. Sci.* **2016**, *362*, 406–417.
[35] H. Wang, Y. Wu, X. Yuan, G. Zeng, J. Zhou, X. Wang, J. W. Chew, *Adv. Mater.* **2018**, *30*, 1704561.
[36] M. Naguib, V. N. Mochalin, M. W. Barsoum, Y. Gogotsi, *Adv. Mater.* **2014**, *26*, 992–1005.
[37] V. Natu, R. Pai, M. Sokol, M. Carey, V. Kalra, M. W. Barsoum, *Chem* **2020**, *6*, 616–630.
[38] J. Halim, M. R. Lukatskaya, K. M. Cook, J. Lu, C. R. Smith, L. -Å Näslund, S. J. May, L. Hultman, Y. Gogotsi, P. Eklund, M. W. Barsoum, *Chem. Mater.* **2014**, *26*, 2374–2381.
[39] Y. Li, H. Shao, Z. Lin, J. Lu, L. Liu, B. Duployer, P. O. Å Persson, P. Eklund, L. Hultman, M. Li, K. Chen, X.-H. Zha, S. Du, P. Rozier, Z. Chai, E. Raymundo-Piñero, P.-L. Taberna, P. Simon, Q. Huang, *Nat. Mater.* **2020**, *19*, 894–899.
[40] W. Sun, S. A. Shah, Y. Chen, Z. Tan, H. Gao, T. Habib, M. Radovic, M. J. Green, *J. Mater. Chem. A* **2017**, *5*, 21663–21668.
[41] J. Xie, X. Wang, A. Li, F. Li, Y. Zhou, *Corros. Sci.* **2012**, *60*, 129–135.
[42] Z. Liu, C. Xu, N. Kang, L. Wang, Y. Jiang, J. Du, Y. Liu, X.-L. Ma, H.-M. Cheng, W. Ren, *Nano Lett.* **2016**, *16*, 4243–4250.
[43] O. Mashtalir, M. Naguib, V. N. Mochalin, Y. Dall'Agnese, M. Heon, M. W. Barsoum, Y. Gogotsi, *Nat. Commun.* **2013**, *4*, 1716.
[44] Q. Zhang, H. Lai, R. Fan, P. Ji, X. Fu, H. Li, *ACS Nano* **2021**, *15*, 5249–5262.
[45] X. Sheng, Y. Zhao, L. Zhang, X. Lu, *Compos. Sci. Technol.* **2019**, *181*, 107710.
[46] M. Boota, M. Pasini, F. Galeotti, W. Porzio, M.-Q. Zhao, J. Halim, Y. Gogotsi, *Chem. Mater.* **2017**, *29*, 2731–2738.
[47] K. Chen, Y. Chen, Q. Deng, S.-H. Jeong, T.-S. Jang, S. Du, H.-E. Kim, Q. Huang, C.-M. Han, *Mater. Lett.* **2018**, *229*, 114–117.
[48] X. Wu, L. Hao, J. Zhang, X. Zhang, J. Wang, J. Liu, *J. Membr. Sci.* **2016**, *515*, 175–188.
[49] Y. Liu, J. Zhang, X. Zhang, Y. Li, J. Wang, *ACS Appl. Mater. Interfaces* **2016**, *8*, 20352–20363.
[50] M. Sajid, H. B. Kim, G. U. Siddiqui, K. H. Na, K. H. Choi, *Sens. Actuators A Phys.* **2017**, *262*, 68–77.
[51] S. Jiao, A. Zhou, M. Wu, H. Hu, *Adv. Sci.* **2019**, *6*, 1900529.
[52] Z. Huang, S. Wang, S. Kota, Q. Pan, M. W. Barsoum, C. Y. Li, *Polymer* **2016**, *102*, 119–126.
[53] S. A. Mirkhani, A. Shayesteh Zeraati, E. Aliabadian, M. Naguib, U. Sundararaj, *ACS Appl. Mater. Interfaces* **2019**, *11*, 18599–18608.
[54] Y. Guo, S. Jin, L. Wang, P. He, Q. Hu, L.-Z. Fan, A. Zhou, *Ceram. Int.* **2020**, *46*, 19550–19556.
[55] J. Shao, J.-W. Wang, D.-N. Liu, L. Wei, S.-Q. Wu, H. Ren, *Polymer* **2019**, *174*, 86–95.
[56] H. Aghamohammadi, N. Amousa, R. Eslami-Farsani, *Synth. Met.* **2021**, *273*, 116695.
[57] L. Gao, C. Li, W. Huang, S. Mei, H. Lin, Q. Ou, Y. Zhang, J. Guo, F. Zhang, S. Xu, H. Zhang, *Chem. Mater.* **2020**, *32*, 1703–1747.
[58] M. Boota, T. Hussain, L. Yang, M. Bécuwe, W. Porzio, L. Barba, R. Ahuja, *Adv. Electron. Mater.* **2021**, *7*, 2001202.
[59] Q. Geng, H. Wang, Y. Wu, L.-P. Lv, S. Chen, W. Sun, Y. Wang, *ChemElectroChem* **2022**, *9*, e202200340.
[60] A. VahidMohammadi, J. Moncada, H. Chen, E. Kayali, J. Orangi, C. A. Carrero, M. Beidaghi, *J. Mater. Chem. A* **2018**, *6*, 22123–22133.
[61] H. Wang, C. Qian, J. Liu, Y. Zeng, D. Wang, W. Zhou, L. Gu, H. Wu, G. Liu, Y. Zhao, *J. Am. Chem. Soc.* **2020**, *142*, 4862–4871.
[62] H. Pang, C. Liu, Y. Bai, W. Li, F. Yang, G. Zhang, *Angew. Chem. Int. Ed.* **2022**, *61*, e202116282.
[63] Y. Liu, Y. He, E. Vargun, T. Plachy, P. Saha, Q. Cheng, *Nanomaterials* **2020**, *10*, 695.
[64] X. Chen, Y. Zhao, L. Li, Y. Wang, J. Wang, J. Xiong, S. Du, P. Zhang, X. Shi, J. Yu, *Polym. Rev.* **2021**, *61*, 80–115.
[65] R. Sun, H.-B. Zhang, J. Liu, X. Xie, R. Yang, Y. Li, S. Hong, Z.-Z. Yu, *Adv. Funct. Mater.* **2017**, *27*, 1702807.
[66] G. Dai, T. Wu, H. Chen, Y. Zhao, *Curr. Opin. Electrochem.* **2021**, *29*, 100745.
[67] C. Zhang, K. Fan, Y. Chen, Y. Wu, C. Wang, *ACS Appl. Electron. Mater.* **2021**, *3*, 1947–1958.
[68] K. Fan, C. Zhang, Y. Chen, Y. Wu, C. Wang, *Chem* **2021**, *7*, 1224–1243.
[69] M. R. Lukatskaya, O. Mashtalir, C. E. Ren, Y. Dall'Agnese, P. Rozier, P. L. Taberna, M. Naguib, P. Simon, M. W. Barsoum, Y. Gogotsi, *Science* **2013**, *341*, 1502–1505.
[70] L. Li, N. Zhang, M. Zhang, X. Zhang, Z. Zhang, *Dalton Trans.* **2019**, *48*, 1747–1756.
[71] M. Boota, B. Anasori, C. Voigt, M.-Q. Zhao, M. W. Barsoum, Y. Gogotsi, *Adv. Mater.* **2016**, *28*, 1517–1522.
[72] A. C. Ezika, E. R. Sadiku, S. S. Ray, Y. Hamam, O. Folorunso, G. J. Adekoya, *J. Inorg. Organomet. Polym.* **2022**, *32*, 1521–1540.
[73] C. Chen, M. Boota, X. Xie, M. Zhao, B. Anasori, C. E. Ren, L. Miao, J. Jiang, Y. Gogotsi, *J. Mater. Chem. A* **2017**, *5*, 5260–5265.
[74] J. S. Seenath, B. P. Biswal, *Adv. Mater. Interfaces* **2021**, *8*, 2101263.
[75] Y. Zhou, Y. Zou, Z. Peng, C. Yu, W. Zhong, *Nanoscale* **2020**, *12*, 20797–20810.
[76] L. Qin, Q. Tao, X. Liu, M. Fahlman, J. Halim, P. O. Å Persson, J. Rosen, F. Zhang, *Nano Energy* **2019**, *60*, 734–742.
[77] X. Zhang, S. Yang, W. Lu, D. Lei, Y. Tian, M. Guo, P. Mi, N. Qu, Y. Zhao, *J. Colloid Interface Sci.* **2021**, *592*, 95–102.
[78] K. Li, X. Wang, S. Li, P. Urbankowski, J. Li, Y. Xu, Y. Gogotsi, *Small* **2020**, *16*, 1906851.
[79] J. P. Chapel, J. F. Berret, *Curr. Opin. Colloid Interface Sci.* **2012**, *17*, 97–105.
[80] J. Zhou, Q. Kang, S. Xu, X. Li, C. Liu, L. Ni, N. Chen, C. Lu, X. Wang, L. Peng, X. Guo, W. Ding, W. Hou, *Nano Res.* **2022**, *15*, 285–295.
[81] W. Yang, B. Huang, L. Li, K. Zhang, Y. Li, J. Huang, X. Tang, T. Hu, K. Yuan, Y. Chen, *Small Methods* **2020**, *4*, 2000434.
[82] Q. Tang, Z. Zhou, P. Shen, *J. Am. Chem. Soc.* **2012**, *134*, 16909–16916.
[83] M. Naguib, J. Come, B. Dyatkin, V. Presser, P.-L. Taberna, P. Simon, M. W. Barsoum, Y. Gogotsi, *Electrochem. Commun.* **2012**, *16*, 61–64.
[84] F. Kong, X. He, Q. Liu, X. Qi, Y. Zheng, R. Wang, Y. Bai, *Electrochim. Acta* **2018**, *265*, 140–150.
[85] X. Wang, J. Chen, D. Wang, Z. Mao, *ACS Appl. Energ. Mater.* **2021**, *4*, 10280–10289.
[86] J. Yang, W. Bao, P. Jaumaux, S. Zhang, C. Wang, G. Wang, *Adv. Mater. Interfaces* **2019**, *6*, 1802004.
[87] Y. Liu, Z. Dai, W. Zhang, Y. Jiang, J. Peng, D. Wu, B. Chen, W. Wei, X. Chen, Z. Liu, Z. Wang, F. Han, D. Ding, L. Wang, L. Li, Y. Yang, Y. Huang, *ACS Nano* **2021**, *15*, 9065–9075.
[88] C. Wei, L. Tan, Y. Zhang, B. Xi, S. Xiong, J. Feng, *ACS Appl. Mater. Interfaces* **2022**, *14*, 2979–2988.
[89] Q. Zhang, Y. Zhang, C. Wei, Y. An, L. Tan, S. Xiong, J. Feng, *J. Power Sources* **2022**, *521*, 230963.
[90] Y. Gao, P. Xue, L. Ji, X. Pan, L. Chen, W. Guo, M. Tang, C. Wang, Z. Wang, *ACS Appl. Mater. Interfaces* **2022**, *14*, 8036–8047.
[91] J. He, M. Shi, J. Jiang, Z. Liu, C. Yang, L. Zhao, C. Yan, *Compos. B. Eng.* **2021**, *222*, 109073.
[92] R. Zhang, Q. Liu, Z. Wang, X. Yang, Y. Guo, *RSC Adv.* **2022**, *12*, 4329–4335.
[93] X. Liang, A. Garsuch, L. F. Nazar, *Angew. Chem. Int. Ed.* **2015**, *54*, 3907–3911; *Angew. Chem.* **2015**, *127*, 3979–3983.
[94] R. Meng, Q. Deng, C. Peng, B. Chen, K. Liao, L. Li, Z. Yang, D. Yang, L. Zheng, C. Zhang, J. Yang, *Nano Today* **2020**, *35*, 100991.
[95] C. Wen, D. Guo, X. Zheng, H. Li, G. Sun, *ACS Appl. Energ. Mater.* **2021**, *4*, 8231–8241.
[96] Y. Zhang, Y. Wu, Y. Liu, J. Feng, *Chem. Eng. J.* **2022**, *428*, 131040.
[97] T. Li, B. Ding, J. Wang, Z. Qin, J. F. S. Fernando, Y. Bando, A. K. Nanjundan, Y. V. Kaneti, D. Golberg, Y. Yamauchi, *ACS Appl. Mater. Interfaces* **2020**, *12*, 14993–15001.
[98] X. Dong, B. Ding, H. Guo, H. Dou, X. Zhang, *ACS Appl. Mater. Interfaces* **2018**, *10*, 38101–38108.
[99] X. Liu, F. Liu, X. Zhao, L.-Z. Fan, *J. Mater.* **2022**, *8*, 30–37.
[100] Y. Xie, X. Xiong, K. Han, *Ionics* **2021**, *27*, 3373–3382.
[101] W. Xu, X. Zhao, J. Tang, C. Zhang, Y. Gao, S.-i. Sasaki, H. Tamiaki, A. Li, X.-F. Wang, *Front. Chem. Sci. Eng.* **2021**, *15*, 709–716.
[102] X. Qi, W. Xu, J. Tang, Y. Xu, Y. Gao, L. Li, S.-i. Sasaki, H. Tamiaki, X. Wang, *J. Mater. Sci.* **2022**, *57*, 9971–9979.

[103] M.-C. Liu, B.-M. Zhang, Y.-S. Zhang, B.-N. Gu, C.-Y. Tian, D.-T. Zhang, Y.-Q. Wang, B. Zhao, Y.-Y. Wang, M.-J. Liu, Y.-J. Yu, K. Zhao, L.-B. Kong, Y.-L. Chueh, *Mater. Today Energy* **2021**, *22*, 100832.
[104] D. Guo, F. Ming, D. B. Shinde, L. Cao, G. Huang, C. Li, Z. Li, Y. Yuan, M. N. Hedhili, H. N. Alshareef, Z. Lai, *Adv. Funct. Mater.* **2021**, *31*, 2101194.
[105] C. Wei, Y. Wang, Y. Zhang, L. Tan, Y. Qian, Y. Tao, S. Xiong, J. Feng, *Nano Res.* **2021**, *14*, 3576–3584.
[106] S. Li, W. Zhang, J. Zheng, M. Lv, H. Song, L. Du, *Adv. Energy Mater.* **2021**, *11*, 2000779.
[107] M. Yan, W.-P. Wang, Y.-X. Yin, L.-J. Wan, Y.-G. Guo, *EnergyChem* **2019**, *1*, 100002.
[108] S. Bai, X. Liu, K. Zhu, S. Wu, H. Zhou, *Nat. Energy* **2016**, *1*, 16094.
[109] S. Zhu, M. Tang, Y. Wu, Y. Chen, C. Jiang, C. Xia, S. Zhuo, B. Wang, C. Wang, *Sustain. Energy Fuels* **2019**, *3*, 142–147.
[110] C. Jiang, M. Tang, S. Zhu, J. Zhang, Y. Wu, Y. Chen, C. Xia, C. Wang, W. Hu, *Angew. Chem. Int. Ed.* **2018**, *59*, 16072–16076.
[111] Q. Zhao, Q. Zhu, Y. Liu, B. Xu, *Adv. Funct. Mater.* **2021**, *31*, 2100457.
[112] H. Pan, X. Huang, R. Zhang, D. Wang, Y. Chen, X. Duan, G. Wen, *Chem. Eng. J.* **2019**, *358*, 1253–1261.
[113] L. Jiao, C. Zhang, C. Geng, S. Wu, H. Li, W. Lv, Y. Tao, Z. Chen, G. Zhou, J. Li, G. Ling, Y. Wan, Q.-H. Yang, *Adv. Energy Mater.* **2019**, *9*, 1900219.
[114] P. Li, H. Lv, Z. Li, X. Meng, Z. Lin, R. Wang, X. Li, *Adv. Mater.* **2021**, *33*, 2007803.

Manuscript received: September 15, 2022
Revised manuscript received: October 20, 2022
Accepted manuscript online: October 24, 2022
Version of record online: November 15, 2022